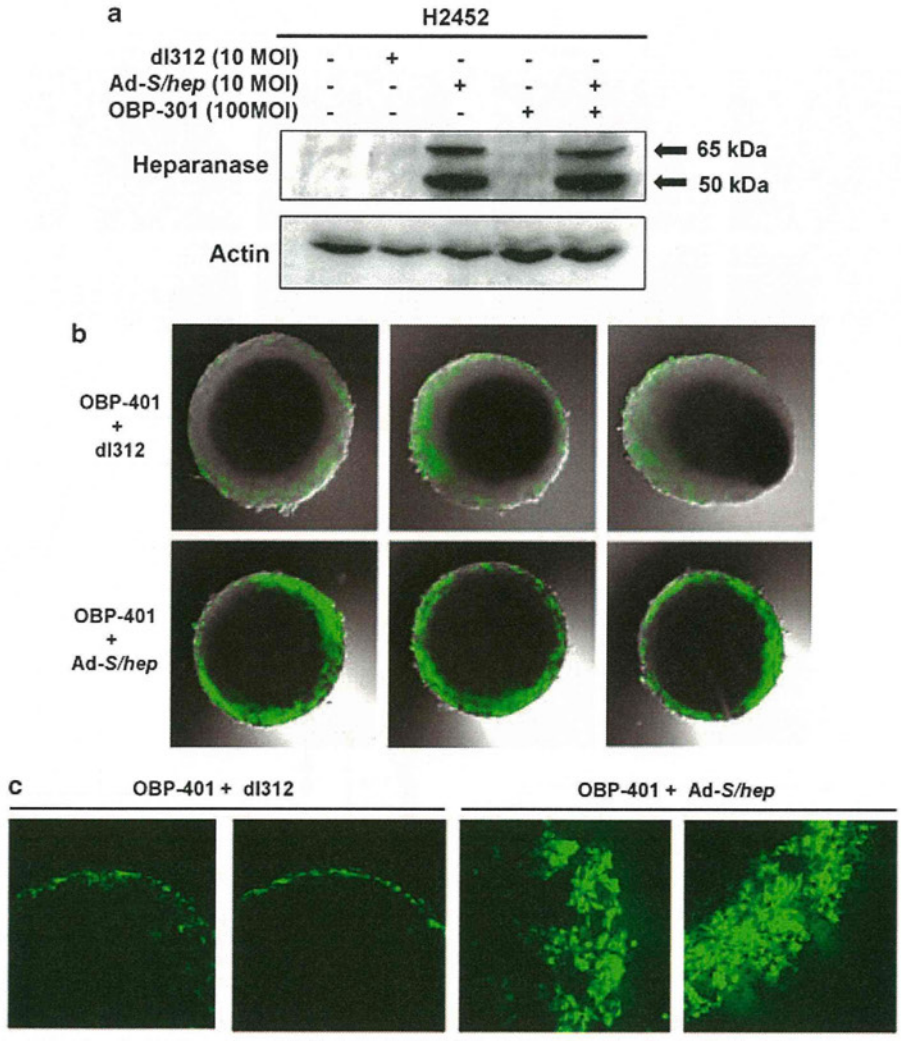

Figure 5 Enhanced penetration of the virus into tumor spheroids by heparanase expression. (**a**) Western blot analysis of human heparanase protein expression in H2452 cells. Cells were infected with either dl312, Ad-*S/hep*, OBP-301 or OBP-301 in combination with Ad-*S/hep* at different multiplicity of infections (MOIs), as indicated. Equivalent amounts of protein obtained from whole cell lysates 30 h after infection were separated by electrophoresis, probed with primary antibodies, and then visualized by using an ECL detection system. Equal loading of samples was confirmed by reprobing with anti-actin antiserum. Both inactive (*Mr* 65 000) and active (*Mr* 50 000) forms of heparanase proteins were detected. (**b**, **c**) Transduction efficiency and viral spread of OBP-401 in combination with Ad-*S/hep* in H2452 tumor spheroids. H2452 tumor spheroids were infected with dl312 (replication-deficient adenovirus) or Ad-*S/hep* at 1×10^3 plaque-forming units (PFU), followed by infection with OBP-401 at 1×10^4 PFU 48 h later. Green fluorescent protein (GFP) expression in each tumor spheroid was assessed with a laser-scanning confocal fluorescent microscope 48 h later. (**b**) Gross imaging of H2452 tumor spheroids. (**c**) Higher magnification to show the surface area of the spheroids.

assessing the levels of virus penetration. Sequential confocal fluorescent microscopy showed that OBP-401 could penetrate and express GFP fluorescence in H2452 spheroids; GFP expression, however, could be detected in the deeper areas of the spheroids in the presence of Ad-*S/hep* (Figure 5b, c). High-magnification images showed that GFP signals were detected only at the spheroid surface after OBP-401 and control dl312 exposure, whereas co-infection of Ad-*S/hep* enhanced the OBP-401 penetration, leading to GFP expression in multiple layers.

Finally, we assessed the combination effect of OBP-301 and Ad-*S/hep* in an orthotopic pleural human mesothelioma model. Intrathoracic injection with 1×10^8 PFU of OBP-301 plus 1×10^7 PFU of Ad-*S/hep* on days 8 and 15 resulted in a significant reduction of tumor weights on day 43 (Figure 6a). This combination therapy showed greater antitumor effects than the therapy with 10^8 PFU of OBP-301 alone. The administration of Ad-*S/hep* alone did not affect tumor weights as compared with the tumors in the mock-treated group. Moreover, only one of the seven (14.3%) mice injected with OBP-301 alone survived over a 12-week observation period, whereas five of the seven (71.4%) mice treated with OBP-301 plus Ad-*S/hep* remained alive (Figure 6b).

Discussion

Malignant pleural mesothelioma is an aggressive neoplasm with a dismal prognosis because of its resistance

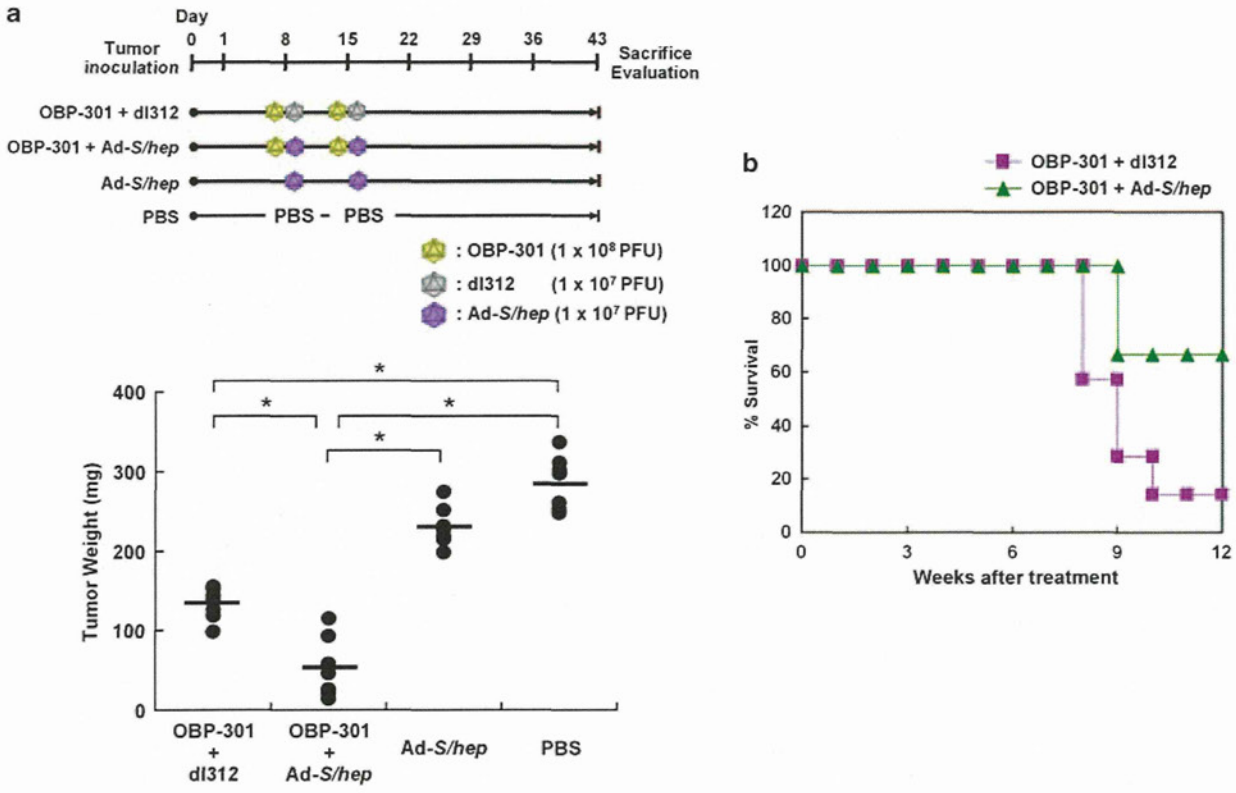

Figure 6 Enhanced antitumor effect of OBP-301 with Ad-*S/hep* in an orthotopic pleural dissemination model. (**a**) Top panel, treatment schedule. Bottom panel, tumor weight of each tumor nodule found in the thoracic spaces after treatment. Treated mice were killed and assessed for pleural dissemination 43 days after tumor inoculation. Closed circles: individual tumor weights. Bars: mean weight. $*P<0.05$. (**b**) Mice bearing H2452 xenografts in the thoracic spaces received intrathoracic administration of either OBP-301 plus dl312 or OBP-301 plus Ad-*S/hep*. Their post-treatment survival was monitored and plotted as a Kaplan–Meier plot.

to therapeutic modalities such as chemotherapy and radiotherapy. An alternative therapeutic option is the use of gene- and vector-based therapies. MPM is characterized by intrathoracic spread, and it is clinically accessible, making it an attractive target for locoregional delivery of genetically engineered viral agents. Replication-competent viral agents can confer specificity of infection and increase viral spread to neighboring tumor cells. Onyx-015, a conditional replication-competent adenovirus lacking the 55-kDa *E1b* gene, may be an effective treatment for human mesothelioma cells retaining wild-type p53 but lacking $p14^{ARF}$ (Ries *et al.*, 2000; Yang *et al.*, 2000, 2001), the targets of Onyx-015, however, are not general and its clinical trials for various types of human malignancies have been discontinued (Goodrum and Ornelles, 1998). In this study, we showed that intrathoracic administration of telomerase-specific oncolytic viruses induced significant antitumor effects against both pre-established and established pleural dissemination of human MPM. Moreover, we found that co-infection of oncolytic adenoviruses with non-replicative adenovirus expressing an ECM-digestive enzyme, heparanase, resulted in a virus distribution into the deeper areas of tumor spheroids, with substantial tumor weight reduction and enhanced efficacy in an orthotopic *in vivo* mesothelioma model.

For the success of gene- and vector-based therapies, it is critical to develop strategies to improve the vector distribution within tumors *in vivo*. Oncolytic viruses can mediate infected cell death, release viral progeny for propagation of infection and induce resultant lysis of neighboring tumor cells. Therefore, these viruses should have a more profound therapeutic efficacy even without particular therapeutic genes when compared with non-replicative viral vectors. Indeed, as human malignant mesothelioma cells express sufficient telomerase activity as well as CAR (Figure 1), most of the disseminated nodules were imaged with GFP fluorescence by intrathoracic administration of GFP-expressing, telomerase-specific OBP-401 in an orthotopic pleural mesothelioma model, which coincided with histologically confirmed mesothelioma (Figure 3). We have recently shown that this OBP-401-mediated GFP-labeling strategy is extremely sensitive to detect disseminated nodules and applicable for the surgical navigation (Kishimoto *et al.*, 2009). A confocal fluorescent imaging system with fibered microprobes showed that OBP-401 could also identify macroscopically invisible tumor tissues, suggesting that OBP-301 might be able to eliminate microscopic dissemination. In fact, local administration of OBP-301 into the thoracic cavity significantly suppressed the disseminated tumor growth (Figure 4). The treatment immediately after mesothelioma

cell inoculation resembles the state of a minimum residual disease after extended surgical excision. Most of the floating mesothelioma cells could be efficiently treated by locoregional OBP-301 administration, resulting in little disseminated tumor nodule formation. Tumor weights, however, increased gradually as the treatment time was delayed (Figure 4c), suggesting that some additional approaches are required to improve the therapeutic efficacy.

Extracellular matrix is a major barrier to macromolecular transport in the tumor interstitium, but digestive enzymes that degrade ECM may overcome the limited spread of viral agents within tumors. Previous studies have shown that protease that degrades multiple ECM components as well as collagenase that digests fibrillar collagen can mediate a broad distribution of virus particles within tumors, leading to enhanced therapeutic efficacy (Kuriyama *et al.*, 2001; McKee *et al.*, 2006). Non-replicating adenovirus vector expressing the matrix metalloproteinase-8 (MMP-8), which effectively degrades collagen-I, was also able to modify a fibrillar collagen substrate to allow oncolytic virus diffusion into tumors (Cheng *et al.*, 2007). More recent studies have also shown that relaxin-expressing, replication-competent adenovirus could increase the virus distribution and show a profound antitumor effect in mice (Kim *et al.*, 2006; Ganesh *et al.*, 2007). Although the most effective enzyme for the promotion of viral penetration into tumor masses has not been determined, we used heparanase, which has a hydrolytic mechanism to cleave glycosidic bonds in the heparan sulfate component of the ECM (McKenzie, 2007).

The expression of functional heparanase degrades the ECM, which in turn improves the uptake and distribution of biological agents including antibodies and viruses (Eikenes *et al.*, 2004). An advantage of heparanase is that other enzymes that are capable of digesting ECM and basement membrane components (such as MMP-2 and MMP-8) can be subsequently induced after heparanase expression. We reported earlier that the over-expression of the heparanase gene upregulated *MMP-2* mRNA expression in human lung cancer cells (Uno *et al.*, 2001). Arterial injury also increased heparanase activity in vascular endothelial cells, which was associated with MMP-2 and MMP-9 activation (Fitzgerald *et al.*, 1999). Therefore, a more prominent virus infiltration through broad ECM degradation with multiple enzymes can be expected by exogenous heparanase expression. The co-infection of Ad-*S/hep* considerably enhanced OBP-401 virus penetration into the multicellular spheroids, mimicking the *in vivo* biology of tumors (Figure 5b, c). Furthermore, combination therapy with OBP-301 and Ad-*S/hep* in an orthotopic murine model significantly reduced the tumor weights of disseminated plural mesothelioma as compared with tumors from mice treated with OBP-301 alone (Figure 6a), suggesting that heparanase-assisted broad virus distribution could mediate a more profound antitumor effect against human malignant mesothelioma.

Our data indicate that this dual virotherapy may be a promising therapeutic strategy for malignant pleural mesothelioma. However, the over-expression of ECM-digesting enzymes may potentially promote the metastasis of tumor cells. MMPs as well as heparanase were detected in many types of human cancer, and their expression has a very active role in tumor invasion and metastasis. Indeed, targeted inhibition of heparanase expression by antisense complementary DNA transfection showed a significant reduction in the invasive and metastatic properties of tumor cells in an animal model (Uno *et al.*, 2001). Short hairpin RNAs that mediated the attenuation of MMP expression also prevented the progression of human tumor cells *in vivo* (Blackburn *et al.*, 2007). Although there is a risk that the metastatic potential of tumor cells may be increased by heparanase expression, we found that the intrathoracic administration of 10^7 PFU of Ad-*S/hep* alone had no apparent effects on the growth of pleural mesothelioma, indicating that this particular dose of the virus appears to be safe (Figure 6a). In the dual-vector system, the two viral loads can be adjusted according to the function of each virus. We showed earlier that telomerase-specific oncolytic viruses and non-replicative adenovirus-expressing functional genes can successfully work together by determining the optimal doses of vectors (Umeoka *et al.*, 2004; Hioki *et al.*, 2008). A single oncolytic virus vector-expressing relaxin inhibits tumor growth and metastasis, however, it may be impossible to reduce the amount of relaxin expression when high doses of the virus are used. In contrast, our dual-vector system of telomerase-specific oncolytic adenovirus in combination with heparanase-expressing replication-deficient adenovirus can be used safely by a fine adjustment of the optimal doses.

In conclusion, our data clearly indicate that telomerase-specific oncolytic adenoviruses have significant therapeutic potential against human malignant pleural mesothelioma *in vitro* and *in vivo*. Moreover, the addition of heparanase-expressing adenovirus significantly enhanced the virus distribution and the antitumor effects of oncolytic adenoviruses. A phase I, dose-escalation study of telomerase-specific oncolytic adenovirus, OBP-301, is currently underway in the United States to assess the treatment feasibility and to characterize its pharmacokinetics in patients with advanced solid tumors (Fujiwara *et al.*, 2008). Phase II studies of telomerase-specific virotherapy in malignant pleural mesothelioma patients are warranted.

Materials and methods

Cell lines and culture conditions

The human mesothelioma cell lines H2052, H2452, H28 and 211H were purchased from American Type Culture Collection (Manassas, VA, USA). H2052 and H2452 cells were cultured as monolayers in RPMI 1640 medium supplemented with 10% fetal bovine serum, 100 units/ml penicillin and 100 mg/ml streptomycin. H28 and 211H were routinely propagated in monolayer culture in RPMI 1640 medium supplemented with 10% fetal bovine serum, 1 mM sodium pyruvate, 100 units/ml penicillin and 100 mg/ml streptomycin. The human non-small-cell lung cancer cell line H1299 was also cultured in RPMI

1640 medium supplemented with 10% fetal bovine serum, 100 units/ml penicillin and 100 mg/ml streptomycin. The normal human lung diploid fibroblast cell line WI38 (JCRB0518) was obtained from the Health Science Research Resources Bank (Osaka, Japan) and grown in Eagle's MEM with 10% fetal bovine serum. The normal human lung fibroblast and the human umbilical vascular endothelial cell line (TaKaRa Biomedicals, Shiga, Japan) were cultured according to the vendors' specifications.

Recombinant adenoviruses
OBP-301 is a telomerase-specific replication-compenent adenovirus variant, in which the hTERT promoter element drives the expression of *E1A* and *E1B* genes linked with internal ribosome entry site (Figure 1a). OBP-301 was modified to create OBP-401 for monitoring viral replicationthe *GFP* gene was inserted under the cytomegalovirus promoter into the E3 region to create OBP-401. Ad-*S/hep* is a replication-deficient adenovirus expressing the human *heparanase* gene under the cytomegalovirus promoter. The E1A-deleted adenovirus dl312 was used as the control adenovirus.

Flow cytometric analysis
A total of 2×10^5 cells were labeled with mouse monoclonal anti-CAR (RmcBUpstate Biotechnology, Lake Placid, NY, USA) for 30 min at 4 °C. Then, the cells were incubated with fluorescein isothiocyanate-conjugated rabbit anti-mouse IgG second antibody (Zymed Laboratories, South San Francisco, CA, USA) and analysed by flow cytometry (FACSCalibur, Becton Dickinson, Mountain View, CA, USA). An isotype-matched normal mouse IgG_1 conjugated to fluorescein isothiocyanate (Serotec, Oxford, UK) was used as a control.

Quantitative real-time PCR analysis of hTERT mRNA
Total RNA from the culture cells was obtained by using the RNeasy Mini Kit (Qiagen, Chatsworth, CA, USA). Approximately 0.1 μg of total RNA was used for reverse transcription. Reverse transcription was performed at 22 °C for 10 min and then at 42 °C for 20 min. The *hTERT* mRNA copy number was determined by real-time quantitative reverse transcription–PCR using a LightCycler instrument and a LightCycler DNA TeloTAGGG hTERT Quantification Kit (Roche Molecular Diagnostics, Indianapolis, IN, USA). Data analysis was performed using the LightCycler software. The ratios normalized by dividing the value of untreated cells were presented for each sample.

Cell viability assay
The XTT assay was performed to measure cell viability. Briefly, cells were seeded at 1×10^3 cells/well in 96-well plates 16–20 h before viral infection and infected with OBP-301 at a MOI of 0, 1, 10 or 50 PFU/cell. Cell viability was determined at the indicated times by using a Cell Proliferation Kit II (Roche Applied Science, Mannheim, Germany) according to the manufacturer's protocol.

Fluorescent microscopy
Human mesothelioma cell lines were infected with 10 MOI of OBP-401 *in vitro*. Expression of the *GFP* gene was assessed and photographed using an IX71 fluorescent microscope (Olympus, Tokyo, Japan) at indicated times.

Western blot analysis
H2452 cells were collected by trypsinization and washed twice in cold phosphate-buffered saline. Cells then were dissolved in lysis buffer containing 50 mM Tris–HCl (pH7.5), 150 mM NaCl, 0.5% Triton X-100, and protease inhibitors (0.2 mM phenylmethylsulfonyl fluoride, 0.2 mM 4-(2-aminoethyl)benzenesul-fonyl-fluoride, 10 μg/ml leupeptin, 10 μg/ml pepstatin, and 1 μg/ml aprotinin).The lysis was performed at 4 °C for 30 min, and then the reaction mixture was centrifuged at 15 000 revolutions per minute. The protein concentration of the supernatant was determined by using the Bio-Rad protein determination method (Bio-Rad, Hercules, CA, USA). Equal amounts (60 μg) of proteins were electrophoresed under reducing conditions on 12% (w/v) polyacrylamide gels. Proteins were electrophoretically transferred to Hy-bond-polyvinylidene diflouride transfer membranes (Amersham, Arlington Heights, IL, USA) and incubated with primary antibodies against heparanase or β-actin, and then peroxidase-linked secondary antibody. An enhanced chemiluminescence Western system (Amersham, Tokyo, Japan) was used to detect secondary probes.

Spheroid culture
Single-cell suspensions of H2452 cells were obtained by trypsinization of monolayer cultures that consisted of 1×10^4 cells seeded on SUMILON Celltight Spheroid (Sumitomo Bakelite Co, Tokyo, Japan) according to the manufacturer's protocol. After formation of small spheroidal aggregates, 1×10^3 PFU of Ad-*S/hep* or dl312 were added to the culture, followed by the addition of 1×10^4 PFU of OBP-401 48 h later. The GFP expression in each tumor spheroid was assessed under the laser-scanning confocal fluorescent microscope (Carl Zeiss, Jena, Germany) 48 h later.

Animal experiments
The experimental protocol was approved by the ethics review committee for animal experimentation of our institution. We used a 27-gauge needle to intrathoracically inject female BALB/c *nu/nu* mice with 100 μl of suspension containing 5×10^6 H2452 cells. The same technique was used for each viral injection into the thoracic space at the indicated time points. Mice were killed and their thoracic spaces were examined macroscopically. Tumor nodules in the thoracic spaces were removed and weighted. *In vivo* GFP fluorescence imaging was also acquired by using a Hamamatsu C5810 three-chip color cooled charged-coupled device camera (Hamamatsu Photonics Systems, Hamamatsu, Japan) and an *in situ* molecular imaging system (Cell~VIZIOMauna Kea Technologies, Paris, France).

Statistical analysis
We used the Student's *t*-test to determine statistically significant differences among the groups. *P*-values <0.05 were considered statistically significant.

Conflict of interest

Yasuo Urata is an employee of Oncolys BioPharma, Inc., the manufacturer of OBP-301 and OBP-401. Toshiyoshi Fujiwara is a consultant of Oncolys BioPharma, Inc.

Acknowledgements

We thank for K Nagai for his helpful discussion. We also thank Y Shirakiya, N Mukai, T Sueishi and M Yokota for their excellent technical support. The Cell~VIZIO system was provided by Mauna Kea Technologies (Paris, France).

References

Alberts AS, Falkson G, Goedhals L, Vorobiof DA, Van der Merwe CA. (1988). Malignant pleural mesothelioma: a disease unaffected by current therapeutic maneuvers. *J Clin Oncol* **6**: 527–535.

Ball DL, Cruickshank DG. (1990). The treatment of malignant mesothelioma of the pleura: review of a 5-year experience, with special reference to radiotherapy. *Am J Clin Oncol* **13**: 4–9.

Blackburn JS, Rhodes CH, Coon CI, Brinckerhoff CE. (2007). RNA interference inhibition of matrix metalloproteinase-1 prevents melanoma metastasis by reducing tumor collagenase activity and angiogenesis. *Cancer Res* **67**: 10849–10858.

Chahinian AP, Pajak TF, Holland JF, Norton L, Ambinder RM, Mandel EM. (1982). Diffuse malignant mesothelioma. Prospective evaluation of 69 patients. *Ann Intern Med* **96**: 746–755.

Chailleux E, Dabouis G, Pioche D, de LM, de Lajartre AY, Rembeaux A *et al.* (1988). Prognostic factors in diffuse malignant pleural mesothelioma. A study of 167 patients. *Chest* **93**: 159–162.

Cheng J, Sauthoff H, Huang Y, Kutler DI, Bajwa S, Rom WN *et al.* (2007). Human matrix metalloproteinase-8 gene delivery increases the oncolytic activity of a replicating adenovirus. *Mol Ther* **15**: 1982–1990.

Connelly RR, Spirtas R, Myers MH, Percy CL, Fraumeni Jr JF. (1987). Demographic patterns for mesothelioma in the United States. *J Natl Cancer Inst* **78**: 1053–1060.

Eikenes L, Bruland OS, Brekken C, Davies CL. (2004). Collagenase increases the transcapillary pressure gradient and improves the uptake and distribution of monoclonal antibodies in human osteosarcoma xenografts. *Cancer Res* **64**: 4768–4773.

Fitzgerald M, Hayward IP, Thomas AC, Campbell GR, Campbell JH. (1999). Matrix metalloproteinase can facilitate the heparanase-induced promotion of phenotype change in vascular smooth muscle cells. *Atherosclerosis* **145**: 97–106.

Fujiwara T, Tanaka N, Numunaitis JJ, Senzer NN, Tong A, Ichimaru D *et al.* (2008). Phase I trial of intratumoral administration of OBP-301, a novel telomerase-specific oncolytic virus, in patients with advanced solid cancer: Evaluation of biodistribution and immune response. *J Clin Oncol* **26**: 3572.

Ganesh S, Gonzalez EM, Idamakanti N, Abramova M, Vanroey M, Robinson M *et al.* (2007). Relaxin-expressing, fiber chimeric oncolytic adenovirus prolongs survival of tumor-bearing mice. *Cancer Res* **67**: 4399–4407.

Goodrum FD, Ornelles DA. (1998). p53 status does not determine outcome of E1B 55-kilodalton mutant adenovirus lytic infection. *J Virol* **72**: 9479–9490.

Hioki M, Kagawa S, Fujiwara T, Sakai R, Kojima T, Watanabe Y *et al.* (2008). Combination of oncolytic adenovirotherapy and Bax gene therapy in human cancer xenografted models. Potential merits and hurdles for combination therapy. *Int J Cancer* **122**: 2628–2633.

Kawashima T, Kagawa S, Kobayashi N, Shirakiya Y, Umeoka T, Teraishi F *et al.* (2004). Telomerase-specific replication-selective virotherapy for human cancer. *Clin Cancer Res* **10**: 285–292.

Kim JH, Lee YS, Kim H, Huang JH, Yoon AR, Yun CO. (2006). Relaxin expression from tumor-targeting adenoviruses and its intratumoral spread, apoptosis induction, and efficacy. *J Natl Cancer Inst* **98**: 1482–1493.

Kishimoto H, Kojima T, Watanabe Y, Kagawa S, Fujiwara T, Uno F *et al.* (2006). *In vivo* imaging of lymph node metastasis with telomerase-specific replication-selective adenovirus. *Nat Med* **12**: 1213–1219.

Kishimoto H, Zhao M, Hayashi K, Urata Y, Tanaka N, Fujiwara T *et al.* (2009). *In vivo* internal tumor illumination by telomerase-dependent adenoviral GFP for precise surgical navigation. *Proc Natl Acad Sci USA* **106**: 14514–14517.

Kuriyama N, Kuriyama H, Julin CM, Lamborn KR, Israel MA. (2001). Protease pretreatment increases the efficacy of adenovirus-mediated gene therapy for the treatment of an experimental glioblastoma model. *Cancer Res* **61**: 1805–1809.

McKee TD, Grandi P, Mok W, Alexandrakis G, Insin N, Zimmer JP *et al.* (2006). Degradation of fibrillar collagen in a human melanoma xenograft improves the efficacy of an oncolytic herpes simplex virus vector. *Cancer Res* **66**: 2509–2513.

McKenzie EA. (2007). Heparanase: a target for drug discovery in cancer and inflammation. *Br J Pharmacol* **151**: 1–14.

Molnar-Kimber KL, Sterman DH, Chang M, Kang EH, ElBash M, Lanuti M *et al.* (1998). Impact of preexisting and induced humoral and cellular immune responses in an adenovirus-based gene therapy phase I clinical trial for localized mesothelioma. *Hum Gene Ther* **9**: 2121–2133.

Murayama T, Takahashi K, Natori Y, Kurumatani N. (2006). Estimation of future mortality from pleural malignant mesothelioma in Japan based on an age-cohort model. *Am J Ind Med* **49**: 1–7.

Price B. (1997). Analysis of current trends in United States mesothelioma incidence. *Am J Epidemiol* **145**: 211–218.

Ries SJ, Brandts CH, Chung AS, Biederer CH, Hann BC, Lipner EM *et al.* (2000). Loss of p14ARF in tumor cells facilitates replication of the adenovirus mutant dl1520 (ONYX-015). *Nat Med* **6**: 1128–1133.

Ruffie P, Feld R, Minkin S, Cormier Y, Boutan-Laroze A, Ginsberg R *et al.* (1989). Diffuse malignant mesothelioma of the pleura in Ontario and Quebec: a retrospective study of 332 patients. *J Clin Oncol* **7**: 1157–1168.

Rusch VW, Piantadosi S, Holmes EC. (1991). The role of extrapleural pneumonectomy in malignant pleural mesothelioma. A Lung Cancer Study Group trial. *J Thorac Cardiovasc Surg* **102**: 1–9.

Ryan CW, Herndon J, Vogelzang NJ. (1998). A review of chemotherapy trials for malignant mesothelioma. *Chest* **113**: 66S–73S.

Sterman DH, Recio A, Carroll RG, Gillespie CT, Haas A, Vachani A *et al.* (2007). A phase I clinical trial of single-dose intrapleural IFN-beta gene transfer for malignant pleural mesothelioma and metastatic pleural effusions: high rate of antitumor immune responses. *Clin Cancer Res* **13**: 4456–4466.

Sterman DH, Recio A, Vachani A, Sun J, Cheung L, DeLong P *et al.* (2005). Long-term follow-up of patients with malignant pleural mesothelioma receiving high-dose adenovirus herpes simplex thymidine kinase/ganciclovir suicide gene therapy. *Clin Cancer Res* **11**: 7444–7453.

Sterman DH, Treat J, Litzky LA, Amin KM, Coonrod L, Molnar-Kimber K *et al.* (1998). Adenovirus-mediated herpes simplex virus thymidine kinase/ganciclovir gene therapy in patients with localized malignancy: results of a phase I clinical trial in malignant mesothelioma. *Hum Gene Ther* **9**: 1083–1092.

Taki M, Kagawa S, Nishizaki M, Mizuguchi H, Hayakawa T, Kyo S *et al.* (2005). Enhanced oncolysis by a tropism-modified telomerase-specific replication-selective adenoviral agent OBP-405 ('Telomelysin-RGD'). *Oncogene* **24**: 3130–3140.

Tango Y, Taki M, Shirakiya Y, Ohtani S, Tokunaga N, Tsunemitsu Y *et al.* (2004). Late resistance to adenoviral p53-mediated apoptosis caused by decreased expression of Coxsackie-adenovirus receptors in human lung cancer cells. *Cancer Sci* **95**: 459–463.

Umeoka T, Kawashima T, Kagawa S, Teraishi F, Taki M, Nishizaki M *et al.* (2004). Visualization of intrathoracically disseminated solid tumors in mice with optical imaging by telomerase-specific amplification of a transferred green fluorescent protein gene. *Cancer Res* **64**: 6259–6265.

Uno F, Fujiwara T, Takata Y, Ohtani S, Katsuda K, Takaoka M *et al.* (2001). Antisense-mediated suppression of human heparanase gene expression inhibits pleural dissemination of human cancer cells. *Cancer Res* **61**: 7855–7860.

Yang CT, You L, Uematsu K, Yeh CC, McCormick F, Jablons DM. (2001). p14(ARF) modulates the cytolytic effect of ONYX-015 in mesothelioma cells with wild-type p53. *Cancer Res* **61**: 5959–5963.

Yang CT, You L, Yeh CC, Chang JW, Zhang F, McCormick F *et al.* (2000). Adenovirus-mediated p14(ARF) gene transfer in human mesothelioma cells. *J Natl Cancer Inst* **92**: 636–641.

Supplementary Information accompanies the paper on the Oncogene website (http://www.nature.com/onc)

In Vivo Biological Purging for Lymph Node Metastasis of Human Colorectal Cancer by Telomerase-Specific Oncolytic Virotherapy

Toru Kojima, MD, Yuichi Watanabe, PhD,†‡ Yuuri Hashimoto, BS,†‡ Shinji Kuroda, MD,* Yasumoto Yamasaki, MD,* Shuya Yano, MD,* Masaaki Ouchi, BS,‡ Hiroshi Tazawa, MD, PhD,† Futoshi Uno, MD, PhD,*† Shunsuke Kagawa, MD, PhD,*† Satoru Kyo, MD, PhD,§ Hiroyuki Mizuguchi, PhD,¶ Yasuo Urata, BS,‡ Noriaki Tanaka, MD, PhD,* and Toshiyoshi Fujiwara, MD, PhD*†*

Background/Objective: The aim of this study was to develop a less invasive way of targeting lymph node metastasis for the treatment of human gastrointestinal cancer. Lymphatic invasion is a major route for cancer cell dissemination, and adequate treatment of locoregional lymph nodes is required for curative treatment in patients with malignancies.

Methods: Human telomerase reverse transcription (hTERT) is the catalytic subunit of telomerase, which is highly active in cancer cells but quiescent in most normal somatic cells. OBP-301 (Telomelysin) is an attenuated adenovirus with oncolytic potency that contains the hTERT promoter element to regulate viral replication. We examined whether OBP-301 injected into the primary tumor might be useful for purging micrometastasis from regional lymph nodes in an orthotopic colorectal cancer model.

Results: OBP-301 was intratumorally injected into HT29 tumors orthotopically implanted into the rectum in BALB/c *nu/nu* mice. By using a highly sensitive quantitative PCR analysis that targets the human-specific *Alu* sequence, we showed that OBP-301 caused viral spread into the regional lymphatic area and selectively replicated in neoplastic lesions, resulting in tumor-cell-specific death in metastatic lymph nodes. Moreover, although the surgical removal of primary tumors increased the tendency of lymph node metastasis, preoperative intratumoral injection of virus significantly reduced lymph node metastasis.

Conclusions: Our results indicate that intratumoral injection of OBP-301 mediates effective in vivo purging of metastatic tumor cells from regional lymph nodes, which may help optimize treatment of human cancer, especially gastrointestinal malignancies.

(*Ann Surg* 2010;251: 1079–1086)

Lymph node status provides important information for both the diagnosis and treatment of human cancer. Lymphatic invasion is a major route for cancer cell dissemination, and lymph node metastasis is a frequent type of recurrence that is associated with a survival disadvantage in many types of cancers.[1–3] Therefore, adequate resection of the locoregional lymph nodes is required for curative treatment in patients with malignancies.[4,5] Extended lymphadenectomy, however, may greatly impair quality of life, especially for patients with early stage epithelial neoplasms in the gastrointestinal tract.[6] Their primary tumors can be removed by new endoluminal therapeutic techniques such as endoscopic submucosal dissection; however, patients with submucosal invasion, lymphovascular infiltration of cancer cells, or undifferentiated histology often become candidates for surgical organ resection with lymphadenectomy, because there is a risk of regional lymph node metastasis, although the frequency is relatively low.[7] Thus, a less invasive way to selectively treat lymph node metastasis would benefit these patients by allowing them to avoid a prophylactic surgery.

Oncolytic viruses that can selectively replicate in tumor cells and lyse infected cells have been extensively investigated as novel anticancer agents.[8–10] These vectors are designed to induce virus-mediated lysis of tumor cells after selective viral propagation within the tumor cell. We previously developed an attenuated adenovirus designated OBP-301 (Telomelysin) that drives the *E1A* and *E1B* genes under the human telomerase reverse transcription (hTERT) promoter.[10–13] The clinical development of OBP-301 as a monotherapy for various solid tumors is currently underway in the United States.[14] We and others have reported that human adenovirus is capable of effective transport into the lymphatic circulation.[15–17] Injection of OBP-401 (TelomeScan), telomerase-specific, replication-competent adenovirus expressing green fluorescent protein (GFP) into primary tumors allows its lymphatic spread, which in turn induces viral replication in metastatic lymph nodes, allowing us to directly image the micrometastases.

In the present study, we explore whether viruses injected into the established primary tumors could traffic to regional lymph nodes and selectively kill metastatic tumor cells in a human colorectal tumor xenograft model. To measure virus-mediated therapeutic efficacy against lymphatic micrometastasis, we established a highly sensitive real-time PCR method targeting human *Alu* sequences.

MATERIALS AND METHODS

Cell Line and Viruses

The human colorectal cancer cell line HT29 was routinely propagated in monolayer culture in McCoy's medium. The recombinant replication-selective, tumor-specific adenovirus vector OBP-301 (Telomelysin), in which the hTERT promoter element drives the expression of *E1A* and *E1B* genes linked with an internal ribosome entry site, was previously constructed and

From the *Division of Surgical Oncology, Department of Surgery, Okayama University Graduate School of Medicine, Dentistry and Pharmaceutical Sciences, Okayama, Japan; †Center for Gene and Cell Therapy, Okayama University Hospital, Okayama, Japan; ‡Oncolys BioPharma, Inc., Tokyo, Japan; §Department of Obstetrics and Gynecology, Kanazawa University School of Medicine, Kanazawa, Japan; and ¶Department of Biochemistry and Molecular Biology, Graduate School of Pharmaceutical Sciences, Osaka University, Osaka, Japan.

Supported in part by grants from the Ministry of Education, Science, and Culture, Japan (to T. F.); grants from the Ministry of Health and Welfare, Japan (to T. F.).

Supplemental digital content is available for this article. Direct URL citations appear in the printed text and are provided in the HTML and PDF versions of this article on the journal's Web site (www.annalsofsurgery.com).

Reprints: Toshiyoshi Fujiwara, MD, PhD, Center for Gene and Cell Therapy, Okayama University Hospital, 2–5-1 Shikata-cho, Okayama 700–8558, Japan. E-mail: toshi_f@md.okayama-u.ac.jp.

ISSN: 0003-4932/10/25106-1079
DOI: 10.1097/SLA.0b013e3181deb69d

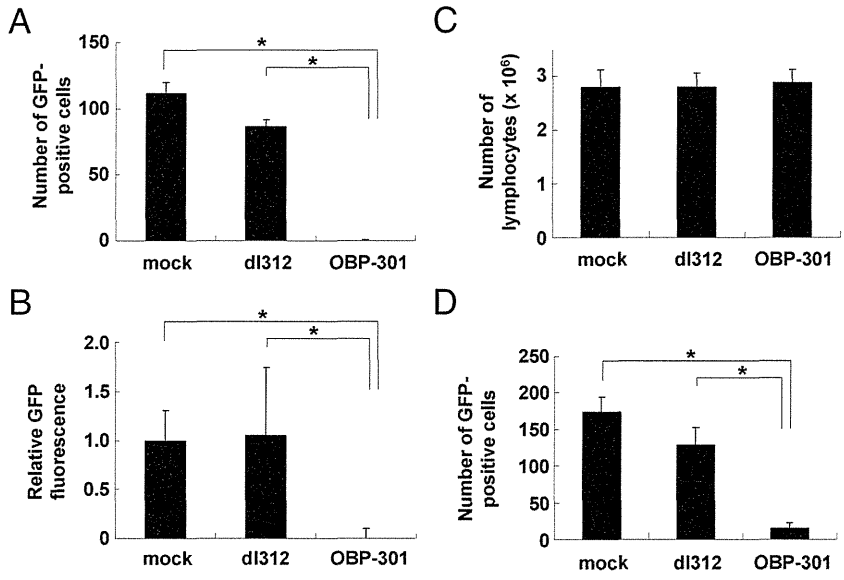

FIGURE 1. In vitro purging effect of OBP-301 infection on HT29 human colorectal cancer cells. We plated 5×10^6 PBMC or mouse splenocytes per well along with 2×10^5 HT29 human colorectal cancer cells. After 24 hours, the mixed culture was infected with 2×10^7 PFU of OBP-301 or dl312 (100 multiplicity of infection [MOI] for HT29 cells) for 96 hours, followed by infection with OBP-401 at 2×10^6 PFU (10 MOI for HT29 cells) to visualize viable HT29 cells (see Figure, Supplemental Digital Content 2, available at: http://links.lww.com/SLA/A39, which illustrates the procedures for in vitro purging experiments). A, The number of GFP-positive, viable HT29 cells was counted in 3 random fields at a magnification of × 200 under the fluorescent microscope. Values represent means ± SEM, and a single asterisk indicates $P < 0.05$ as compared with the other groups. B, The intensity of GFP fluorescence in each treatment group was also measured by using a fluorescence microplate reader. Values are relative to mock (mock = 1) and represent means ± SEM. A single asterisk indicates $P < 0.05$. C, Toxicity of OBP-301 infection was assessed for human lymphocytes. A total of 5×10^6 PBMCs were exposed to 2×10^7 PFU of OBP-301 or dl312 for 96 hours, and their viability was then determined by trypan blue exclusion. D, An efficient purging effect of OBP-301 on HT29 cells in mouse splenocytes. To mimic the animal experiments in vitro, HT29 cells mixed with splenocytes from BALB/c *nu/nu* mice were exposed to OBP-301 or dl312 for 96 hours, followed by OBP-401 infection. The number of cells positive for GFP was counted as described above, and presented as the mean ± SEM. A single asterisk indicates $P < 0.05$.

characterized.[11] OBP-401 (TelomeScan) is a telomerase-specific, replication-competent adenovirus variant in which the replication cassette and *GFP* gene under the control of the cytomegalovirus promoter were inserted into the E3 region for monitoring viral replication[15] (see Figure, Supplemental Digital Content 1, online only, available at http://links.lww.com/SLA/A38, which illustrates schematic DNA structures of telomerase-specific viruses). The *E1A*-deleted adenovirus vector lacking a cDNA insert (dl312) was also used as a control vector.

In Vitro Purging Experiments

For in vitro purging studies, peripheral blood samples were drawn from healthy volunteers, and mononuclear cells were isolated by sedimentation over Ficoll-Hypaque. Mouse spleens were removed aseptically and gently crushed with the flat end of a sterile syringe. The cells were passed through nylon mesh and then placed in buffered ammonium chloride solution to produce osmotic lysis of erythrocytes. We plated peripheral blood mononuclear cells (PBMC) or mouse splenocytes per well along with HT29 cells. The purging effect was assessed with an Eclipse TS-100 fluorescent microscope (Nikon, Tokyo, Japan) by counting the number of GFP-positive cells 24 hours after OBP-401 infection (see Figure, Supplemental Digital Content 2, online only, available at http://links.lww.com/SLA/A39, which illustrates the procedures for in vitro purging experiments). GFP fluorescence was also measured by using a fluorescence microplate reader (DS Pharma Biomedical, Osaka, Japan) with excitation/emission at 485 nm/528 nm.

Xenograft Model of Lymph Node Metastasis

The experimental protocol was approved by the Ethics Review Committee for Animal Experimentation of our institution. The implantation procedures for human rectal cancer xenografts were described previously.[15] Cell suspensions of HT29 cells at a density of 5×10^6 cells in 100 μL of Matrigel (BD Biosciences, Bedford, MA) were slowly injected into the submucosal layer of the rectum by using a 27-gauge needle. For pathologic evaluation of lymph node metastasis, mice were killed and all para-aortic or iliac lymph nodes were isolated and stained with hematoxylin and eosin.

In Vivo Fluorescence Imaging

In vivo GFP fluorescence imaging was acquired by illuminating the animal with a Xenon 150 W lamp. The re-emitted fluorescence was collected through a long pass filter on a Hamamatsu C5810 3-chip color cooled charged-coupled device (CCD) camera (Hamamatsu Photonics Systems, Hamamatsu, Japan). Abdominal images were also obtained during laparotomy with the IVIS CCD camera and analyzed with Living Image 2.20.1 software (Xenogen/Caliper Life Sciences, Hopkinton, MA) for the quantification of lymph node metastasis.

Quantitative Real-Time PCR Analysis

To measure the amounts of human tumor cells in mouse lymph nodes, we applied a previously described quantitative PCR assay that uses primer sets to amplify human *Alu* sequences present in mouse lymph node DNA extracts. Genomic DNA was extracted

from mixed cell cultures or harvested tissues by using a QIAamp DNA Mini Kit (Qiagen Inc., Valencia, CA). To detect human cells in the mouse tissues, a set of human *Alu* primers (sense: 5′-CTG AGG TCA GGA GTT CGA G-3′; and antisense: 5′-TCA AGC GAT TCT CCT GCC-3′) were designed. We performed the quantitative real-time PCR assay by using a LightCycler instrument (Roche Molecular Biochemicals, Indianapolis, IN). PCR amplification began with a 120-second denaturation step at 95°C and then 30 cycles of denaturation at 95°C for 30 seconds, annealing at 63°C for 30 seconds, and extension at 72°C for 30 seconds. We also amplified the mouse *GAPDH* genomic DNA sequence with mouse *GAPDH* primers (sense: 5′-CCA CTC TTC CAC CTT CGA T-3′; and antisense: 5′-CAC CAC CCT GTT GCT GTA-3′) by using the same PCR conditions described for *Alu*. The amounts of *E1A* DNA of OBP-301 and OBP-401 were measured as previously described. The sequences of specific primers used for *E1A* were as follows: sense: 5′-CCT GTG TCT AGA GAA TGC AA-3′; and antisense: 5′-ACA GCT CAA GTC CAA AGG TT-3′. PCR amplification of genomic DNA extracted from mouse lymph nodes was performed with precycling heat activation of DNA polymerase at 95°C for 600 seconds, followed by 40 cycles of denaturation at 95°C for 10 seconds, annealing at 58°C for 15 seconds, and extension at 72°C for 8 seconds. Data analysis was performed with LightCycler Software (Roche Molecular Biochemicals).

Statistical Analysis

We used the Student 2-tailed *t* test to identify statistically significant differences between groups. Results are reported as mean ± SEM. *P* values less than 0.05 were considered statistically significant.

RESULTS

In Vitro Purging of Human Colorectal Cancer Cells by Telomerase-Specific Oncolytic Adenovirus

To examine whether telomerase-specific oncolytic adenovirus can selectively kill human tumor cells among the millions of lymphocytes in lymph nodes, HT29 human colorectal cancer cells were mixed with PBMC from healthy donors and purged in vitro with OBP-301 for 3 days. Viable HT29 cells were then visualized with GFP fluorescence by OBP-401 infection for 24 hours (see Figure, Supplemental Digital Content 2, online only, available at http://links.lww.com/SLA/A39, which illustrates the procedures for in vitro purging experiments). No GFP-positive viable HT29 cells were detected at 3 days postpurging with OBP-301, whereas infection with replication-deficient control adenovirus dl312 had no significant effects on the viability of HT29 cells (Fig. 1A) (see Figure, Supplemental Digital Content 2, online only, available at: http://links.lww.com/SLA/A39, which demonstrates in vitro purging effect of OBP-301 infection). The purging efficacy of OBP-301 was also confirmed by measuring the relative GFP expression of samples by using a fluorescence microplate reader (Fig. 1B). Neither OBP-301 nor dl312 infection affected the viability of PBMC, confirming the safety of OBP-301 to normal human lymphocytes (Fig. 1C). Next, we determined if human tumor cells mixed with mouse lymphocytes obtained from the spleen would be sensitive to OBP-301 treatment. As expected, purging with OBP-301 significantly reduced the number of viable HT29 cells in mouse splenocytes compared with mock- or dl312-treated samples (Fig. 1D).

In Vivo Lymphatic Spread of Virus on Regional Lymph Nodes

To verify that oncolytic adenoviruses traffic through the lymphatics to the regional lymph nodes, we used an orthotopic mouse model of human rectal cancer with spontaneous lymph node metastasis. We first determined whether the regional lymphatic system, including lymphatic vessels and lymph nodes, could be assessed by injecting dye into the primary tumors. Intense blue staining was detected in regional lymph nodes as early as 1 minute after injection of indigo carmine blue dye into the primary rectal tumors, indicating that the injected solution could rapidly enter the intratumoral lymphatics, which provides a route from the primary tumor to draining lymph nodes (Fig. 2A). Five days after OBP-401 injection into the primary tumors, we also detected GFP expression in both primary rectal tumors and metastatic lymph nodes under the laparotomy by using a 3-chip CCD optical imaging system (Fig. 2B).

To further evaluate the selective replication ability of telomerase-specific oncolytic adenovirus in metastatic lymph nodes, we measured the relative amounts of *E1A* DNA by quantitative real-time PCR analysis. The metastatic GFP-positive lymph nodes con-

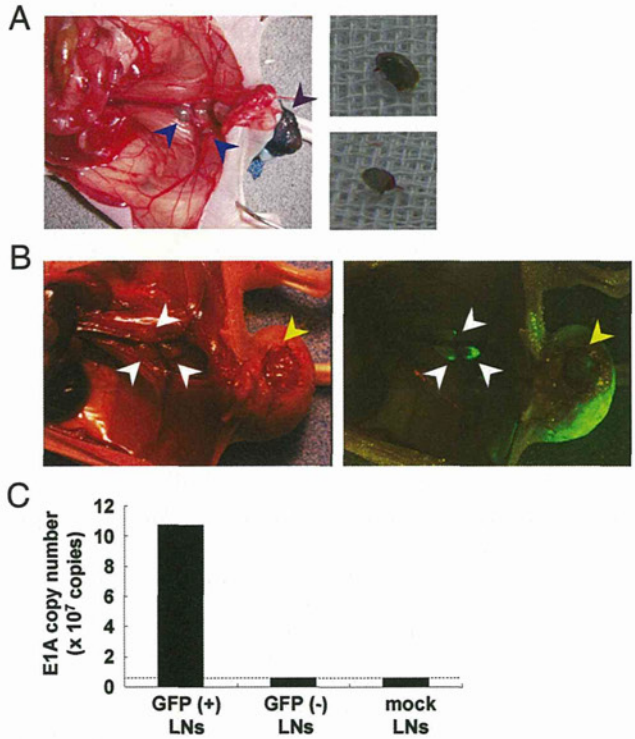

FIGURE 2. In vivo lymphatic spread of virus on regional lymph nodes. A, A lymphatic drainage pattern in an orthotopic xenograft of human HT29 cells. The abdominal cavity was photographed 1 minute after injection of 1% indigo carmine blue dye into an established orthotopic HT29 tumor. Arrowheads indicate the lymph nodes stained with blue dye. Gross appearance of the abdominal cavity (left) and excised lymph nodes (right). B, Five days after intratumoral injection of 1×10^8 PFU of OBP-401, HT29 tumor-bearing *nu/nu* mice were assessed for lymph node metastasis during laparotomy. Macroscopic (left) and fluorescent (right) images. Primary tumor (yellow arrowhead) and metastatic lymph nodes (white arrowheads) are shown. C, Assessment of viral replication in metastatic lymph nodes. GFP-positive and -negative lymph nodes were harvested from mice with HT29 tumor xenografts 5 days after injection of 1×10^8 PFU of OBP-401 and then subjected to real-time quantitative PCR assay to quantify the amounts of viral *E1A* copy number. The value in mock-infected lymph nodes is indicated with a dotted line as a baseline level.

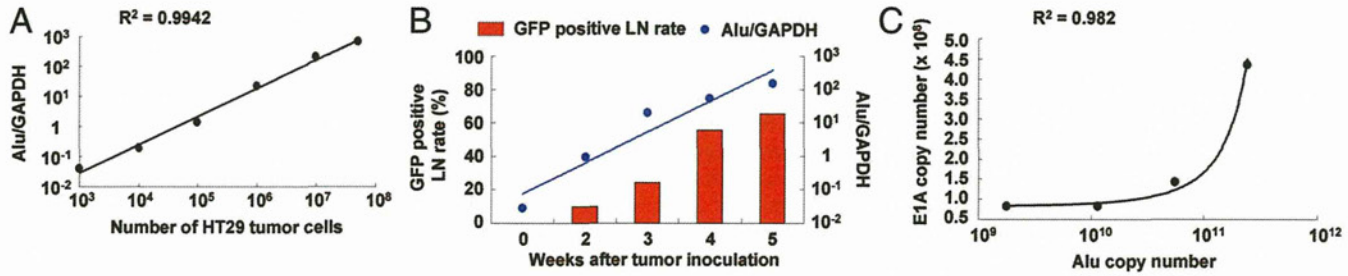

FIGURE 3. Detection and quantification of human cancer cells in mouse tissues with a quantitative real-time *Alu*PCR analysis. A, Generation of a standard curve. Mouse splenocytes (5×10^7 cells) were spiked with serially diluted HT29 human colorectal cancer cells. Genomic DNA was extracted from the mixtures and then subjected to the quantitative amplification (see Figure, Supplemental Digital Content 4A, available at: http://links.lww.com/SLA/A41, which illustrates schematic procedures of detection and quantification of human cancer cells in mouse splenocytes). The *Alu*/*GAPDH* ratios *versus* the numbers of spiked HT29 cells are presented. Regression analysis yielded a correlation coefficient of $R^2 = 0.9942$. The data are representative of 3 separate experiments. B, Quantitative analysis of spontaneous lymph node metastasis. Genomic DNA was extracted from the lymph nodes of mice bearing human HT29 tumor xenografts at the indicated time points after tumor inoculation and analyzed with the quantitative *Alu*PCR assay (see Figure, Supplemental Digital Content 4B, available at: http://links.lww.com/SLA/A41, which illustrates schematic procedures of detection and quantification of human cancer cells in mouse tissues). Metastatic lymph nodes were simultaneously visualized by injecting 1×10^8 PFU of OBP-401 into the primary tumors 5 days before lymph node isolation. C, The viral *E1A* copy numbers were also determined in genomic DNA extracted from isolated lymph nodes by the quantitative real-time PCR method and plotted *versus* the *Alu* copy numbers.

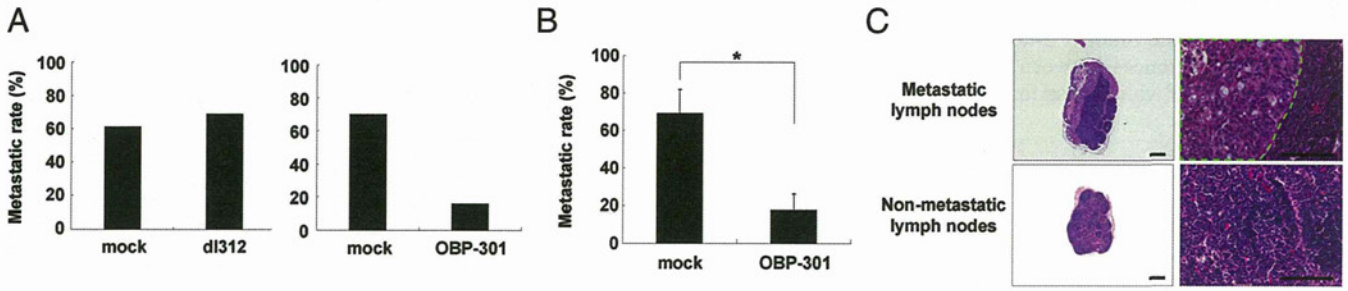

FIGURE 4. Histologic evaluation of selective antitumor effect of OBP-301 delivered into primary tumors on lymphatic metastasis in a colorectal cancer xenograft model. Mice bearing orthotopic HT29 tumors received 3 courses of intratumoral injections of 1×10^8 PFU of OBP-301 or dl312 every 2 days beginning on day 14 after the tumor inoculation. A, On day 35, we harvested a total of 23 to 29 lymph nodes from 5 to 8 mice per group, stained them with hematoxylin and eosin, and calculated metastatic rates. B, In a separate experiment, metastatic rates were histologically determined in individual mice and averaged with S.E.M. ($n = 8$). A single asterisk denotes statistical significance ($P < 0.05$) as compared with the mock group. C, Paraffin-embedded sections of lymph nodes with or without metastatic foci were obtained 35 days after tumor cell implantation and stained with hematoxylin and eosin. Left, ×40 magnification; right, ×200 magnification. Scale bar, 100 μm. The area with metastatic HT29 cells is indicated with the green dotted line.

tained more than 10^8 copies of OBP-401, whereas the number of viral genomes was at the baseline level in nonmetastatic GFP-negative lymph nodes (Fig. 2C). The trafficking and replication ability of the virus was also confirmed in an orthotopic head and neck cancer xenograft model (see Figure, Supplemental Digital Content 3, online only, available at: http://links.lww.com/SLA/A40, which demonstrates OBP-401 virus spread delivered into primary tumors).

Establishment of Highly Sensitive Quantitative Detection Assay for Lymph Node Metastasis

To achieve the highest sensitivity for detecting metastatic human tumor cells in mouse lymph nodes, we applied a novel quantitative real-time PCR assay that uses primer sets to amplify the consensus human *Alu* sequence.[18–20] *Alu* repeat sequences are specific to all human cells and are completely absent in mouse tissues.[21] To test the sensitivity and range of the assay, mouse splenocytes obtained from athymic *nu/nu* mice were spiked with variable numbers of HT29 human colorectal cancer cells in vitro (see Figure, Supplemental Digital Content 4A, online only, available at: http://links.lww.com/SLA/A41, which illustrates schematic procedures of detection and quantification of human cancer cells in mouse splenocytes). The total genomic DNA was extracted from the mixtures and subjected to quantitative *Alu*PCR. We also used the human *GAPDH* gene as an internal control to normalize the *Alu* signal in each sample. By plotting the *Alu*/*GAPDH* ratio as a function of the number of spiked tumor cells, a standard curve could be generated with a linear range between 10^3 and 10^8 cells, and regression analysis of the *Alu*/*GAPDH* ratio *versus* the number of expected tumor cells yielded a correlation coefficient of $R^2 = 0.9942$ ($P < 0.01$) (Fig. 3A). These results suggest that the *Alu*/*GAPDH* ratio reflects the actual human tumor cells among mouse splenocytes.

To verify the accuracy and sensitivity of the assay in vivo, we extracted DNA from total lymph nodes at different time points after the orthotopic implantation of HT29 cells and subjected the DNA to the *Alu*PCR analysis (see Figure, Supplemental Digital Content 4B,

online only, available at: http://links.lww.com/SLA/A41, which illustrates schematic procedures of detection and quantification of human cancer cells in mouse tissues). Then, we compared the *Alu/GAPDH* ratios and the metastatic rates determined with GFP expression by injection of OBP-401 into the primary rectal tumors 5 days before lymph node isolation. The *Alu/GAPDH* ratio showed a linear increase in a time-dependent manner, as the GFP-positive metastatic lymph node rate gradually increased (Fig. 3B). By calculating the estimated number of tumor cells according to the standard curve, we also demonstrated the time-dependent logarithm increase in metastatic human tumor cells in mouse lymph nodes (see Figure, Supplemental Digital Content 5, online only, available at: http://links.lww.com/SLA/A42, which demonstrates quantitative analysis of time-dependent development of spontaneous lymph node metastasis). Moreover, when HT29 tumor-bearing mice received a single intratumoral injection of OBP-401, the number of *Alu* copies was clearly correlated with the number of *E1A* copies in isolated mouse lymph nodes ($R^2 = 0.982$, $P < 0.01$), because telomerase-specific oncolytic adenovirus replicates only in metastatic tumor cells (Fig. 3C).

Histologic Evaluation of the In Vivo Antitumor Effect of Virus on Lymph Node Metastasis

We next examined the in vivo antitumor effect of OBP-301 injected into the primary tumors on the regional lymph node metastasis. Mice bearing orthotopic HT29 rectal tumors with a diameter of 7 to 10 mm received 3 courses of intratumoral injections of 10^8 plaque forming units (PFU) of OBP-301 or dl312, or PBS (mock treatment), every 2 days beginning on day 14 after the tumor inoculation. Histopathological examination of the excised total lymph nodes on day 35 showed that OBP-301 treatment considerably reduced the metastatic rates compared with that of mock-treated group, although replication-deficient dl312 had no apparent effects (Fig. 4A) (see Table, Supplemental Digital Content 6, online only, available at: http://links.lww.com/SLA/A43, which demonstrates histologic evaluation of antitumor effect of OBP-301 on lymph node metastasis). We also confirmed that OBP-301 significantly lowered the lymph node metastatic rates by averaging the histologically determined metastasis rates in individual mice ($P < 0.05$) (Fig. 4B). Representative histopathological images of lymph nodes with or without metastatic foci composed of HT29 tumor cells are shown in Figure 4C.

Quantitative Evaluation of the In Vivo Antitumor Effect of Virus on Lymph Node Metastasis

By using a highly sensitive quantitative *Alu*PCR assay, we next investigated the antitumor effect of OBP-301 injected into the primary tumors on lymph node metastasis, which might be histopathologically undetectable. Mice received 3 courses of injections of 10^8 PFU of OBP-301, 10^8 PFU of dl312, or PBS (mock treatment) into orthotopic HT29 rectal tumors every 2 days beginning on day 14 after tumor inoculation. The *Alu* real-time PCR assay of isolated lymph nodes on day 35 demonstrated that mice treated with OBP-301 exhibited significantly fewer metastatic tumor cells as compared with dl312- or mock-treated mice (Fig. 5A). A more profound antitumor effect was achieved by increasing the number of injection cycles from 3 to 5 (see Figure, Supplemental Digital Content 7, online only, available at: http://links.lww.com/SLA/A44, which demonstrates quantitative analysis of antitumor effect of OBP-301 on lymph node metastasis). As expected, regional lymph nodes obtained from OBP-301-treated mice contained more *E1A* copies than the lymph nodes of mock-treated mice (Fig. 5B), suggesting that intratumorally delivered OBP-301 could spread and selectively replicate in metastatic lymph nodes.

We also used OBP-401 and the IVIS imaging system to assess the in vivo antitumor effect of OBP-301 on lymph node metastasis. After 14 days of orthotopic implantation of HT29 cells, OBP-301 (1×10^8 PFU/body) was administered intratumorally for 5 cycles. We then used the IVIS imaging system to explore the abdominal cavity at laparotomy on day 35 following a single injection of OBP-401 (1×10^8 PFU/body) into HT29 rectal tumors on day 30 (see Figure, Supplemental Digital Content 8, online only, available at: http://links.lww.com/SLA/A45, which illustrates schematic procedures of quantitative imaging of lymph node metastasis by the IVIS system). The number of GFP-positive lymph nodes and the GFP signal levels of individual lymph nodes were much higher in mock-treated control mice than in OBP-301-treated mice (Fig. 6A). Indeed, the sum of GFP fluorescence intensity in the abdominal cavity was significantly lower in mice treated with OBP-301 as compared with the mock-treated group, confirming the in vivo biologic purging effect of OBP-301 (Fig. 6B).

Preoperative Purging Efficacy of Oncolytic Virotherapy against Lymph Node Metastasis

To compare the local control rates of virotherapy and radiotherapy for lymph node metastasis, mice bearing orthotopic HT29 tumors were treated with an intratumoral injection of 10^8 PFU of

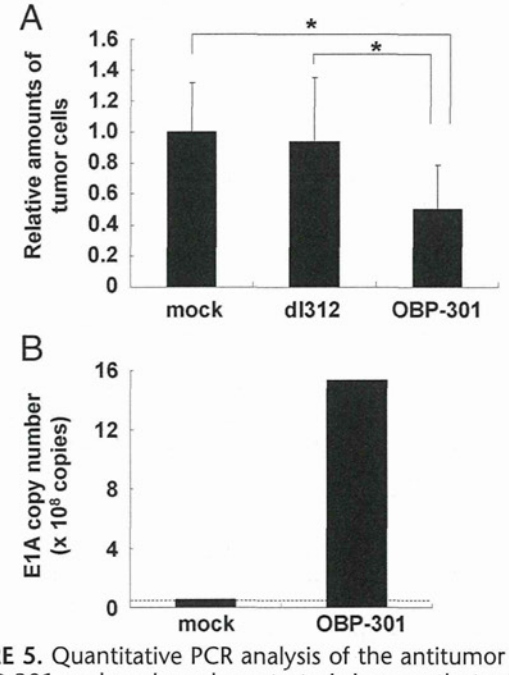

FIGURE 5. Quantitative PCR analysis of the antitumor effect of OBP-301 on lymph node metastasis in an orthotopic colorectal cancer xenograft model. A, Mice with established orthotopic HT29 tumors were treated with intratumoral injection of 1×10^8 PFU of OBP-301 or dl312 every 2 days for 3 cycles starting on day 14 after tumor inoculation. Lymph nodes were harvested on day 35, and then DNA was extracted and subjected to the quantitative *Alu*PCR analysis. The number of metastatic tumor cells is defined as the *Alu/GAPDH* ratio relative to that of the mock-treated sample (mock = 1). Data are shown as the mean ± SEM of 3 separate experiments. Statistical significance was defined as $P < 0.05$ (single asterisk). B, Genomic DNA extracted from lymph nodes of mice that received OBP-301 or PBS was also analyzed with real-time PCR targeting *E1A* to quantify the viral replication. A dotted line represents the baseline level.

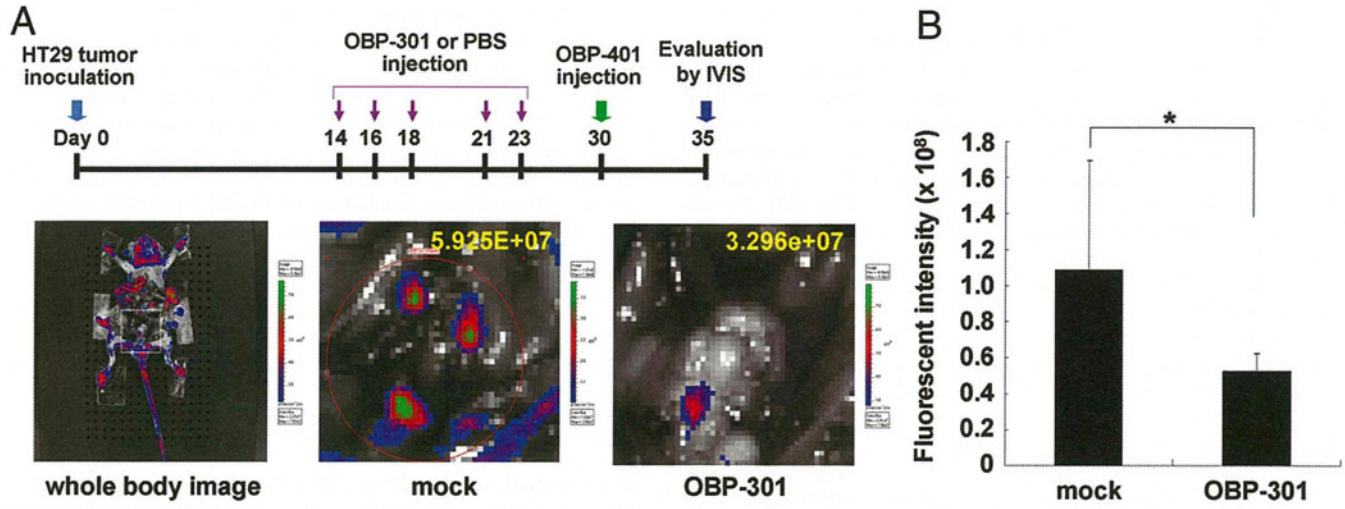

FIGURE 6. Quantitative imaging of lymph node metastasis to evaluate the antitumor effect of OBP-301 in an orthotopic colorectal cancer xenograft model. A, Quantitative imaging of lymph node metastasis by the IVIS system. Mice bearing HT29 xenograft tumors were treated with 5 cycles of intratumoral delivery of 1×10^8 PFU of OBP-301, followed by injection of OBP-401 (10^8 PFU) into HT29 tumors. Five days later, mice were killed and GFP expression was quantitated at laparotomy by IVIS camera (see Figure, Supplemental Digital Content 8, available at: http://links.lww.com/SLA/A45, which illustrates schematic procedures of quantitative imaging of lymph node metastasis by the IVIS system). B, GFP expression was measured as the mean photon flux in mock- and OBP-301-treated groups. A single asterisk indicates a statistically significant difference as compared with the mock-treated group.

OBP-301 or lower hemi-body ionizing radiation at a dosage of 3.3 Gy every 2 days for 3 cycles starting 14 days after tumor inoculation (see Figure, Supplemental Digital Content 9, online only, available at: http://links.lww.com/SLA/A46, which illustrates schematic procedures of quantitative PCR evaluation). The *Alu*PCR analysis of isolated lymph nodes at day 35 demonstrated that both intratumoral administration of OBP-301 and radiation equally resulted in a significant suppression of lymph node metastasis compared with mock-treated mice (Fig. 7A). However, regarding the adverse effects, the lower hemi-body irradiation targeting the regional para-aortic lymph nodes induced a significant body weight loss in mice approximately 10 to 14 days after treatment, whereas there were no apparent adverse effects in mice injected with OBP-301 during the observation period (data not shown). These results suggest that oncolytic virotherapy is less toxic than regional radiotherapy, although the antitumor effects of both approaches may be equivalent.

Finally, we examined whether preoperative intratumoral administration of OBP-301 had an antitumor effect against lymph node metastasis following the primary tumor resection. Mice bearing orthotopic HT29 tumors received intratumoral injections of 10^8 PFU of OBP-301 every 2 days for 3 cycles starting 10 days after tumor inoculation. After primary rectal tumors were surgically removed on day 15, regional para-aortic lymph nodes were isolated on day 35, and then subjected to the *Alu*PCR analysis (see Figure, Supplemental Digital Content 9, online only, available at: http://links.lww.com/SLA/A46, which illustrates schematic procedures of quantitative PCR evaluation). The surgical resection of primary tumors caused considerable enhancement of lymph node metastasis; the preoperative treatment with OBP-301, however, not only inhibited the increase of lymphatic metastasis, but also significantly reduced lymph node metastasis compared with mock-treated mice (Fig. 7B). Images of representative mice before and after primary tumor resection are shown in Figure 7C. As implanted HT29 cells formed submucosal tumors with a solid architecture, tumors could be successfully excised with an incision in the anorectal wall (Fig. 7D).

DISCUSSION

Lymph node metastases represent an aggressive tumor behavior and are associated with a high rate of regional recurrence, which portends a poor outcome and may produce marked morbidity.[1–3] Therefore, it would be clinically beneficial to eliminate or prevent lymph node metastasis to yield a better prognosis for cancer patients. Despite advances in surgical procedures of extended lymphadenectomy,[4,5] a more effective and less invasive management of lymphatic metastasis is needed. Here we describe a new, simple, and robust strategy that uses the telomerase-specific, replication-selective, oncolytic adenovirus OBP-301 to suppress tumor cell dissemination to regional lymph nodes in an orthotopic human colorectal cancer xenograft model.

The therapeutic potential of viral agents against primary tumors as well as their systemic biodistribution targeting distant metastases has been intensively investigated.[8,9,22] Few studies, however, have examined the ability of the virus to traffic to the regional draining lymph nodes. Recently, Burton et al showed that replication-deficient adenovirus could be successfully transported to the regional lymph nodes and noninvasively detect metastasis by expressing the prostate-specific reporter gene in an orthotopic prostate xenograft.[17] We have also previously demonstrated that intratumoral injection of the telomerase-specific, replication-selective, GFP-expressing adenovirus OBP-401 could efficiently visualize metastatic lymph nodes with GFP fluorescence signals in human cancer xenograft models.[15,23] Although these previous studies suggest the possible application of the adenovirus vectors as a lymphotropic agent for the treatment of lymph node metastasis, this effect has not been tested prior to the present study.

In vitro purging experiments demonstrated that OBP-301 infection could selectively eliminate human tumor cells in the presence of human or mouse lymphocytes (Fig. 1). We used OBP-401 to visualize viable human tumor cells after purging with OBP-301, as we have previously shown the high sensitivity and specificity

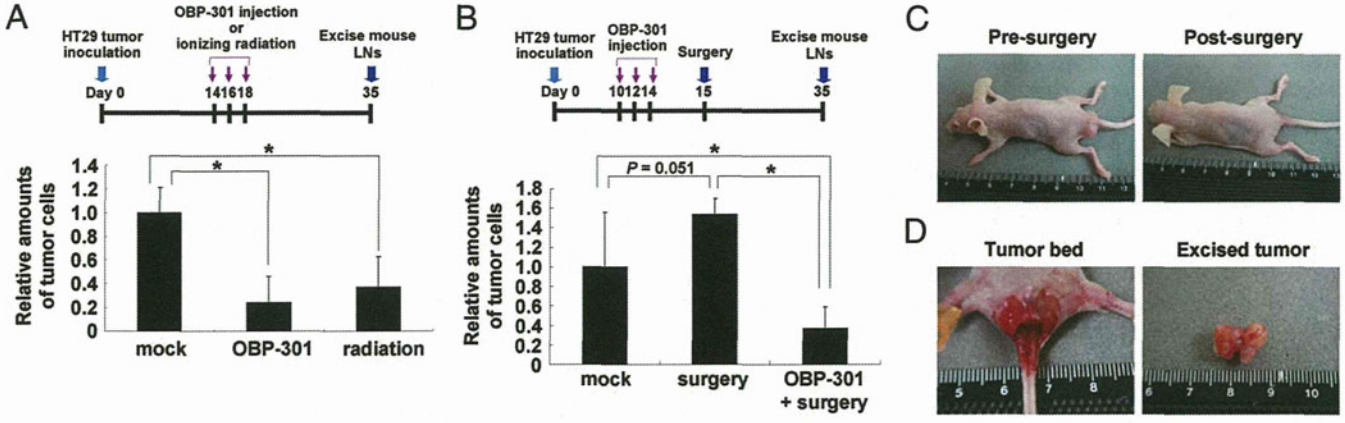

FIGURE 7. Comparative analysis of OBP-301 virotherapy with radiotherapy and surgery. A, In vivo purging effects of regional therapy with OBP-301 or ionizing irradiation on lymph node metastasis. Mice bearing HT29 xenograft tumors received 3 cycles of either intratumoral administration of OBP-301 (10^8 PFU) or lower hemibody irradiation starting at day 14 after tumor inoculation. Radiation was given every 2 days in 3.3-Gy fractions for a total dose of 10 Gy/mouse (see Figure, Supplemental Digital Content 9, available at: http://links.lww.com/SLA/A46, which illustrates schematic procedures of quantitative PCR evaluation). The number of metastatic tumor cells in mouse lymph nodes isolated on day 35 is defined as the *Alu/GAPDH* ratio relative to that of the mock-treated sample (mock = 1). Data are shown as the mean ± SEM of 3 separate experiments. Statistical significance was defined as $P < 0.05$ (single asterisk). (B) Preoperative purging effect of OBP-301 on lymph node metastasis. HT29 tumor-bearing mice were intratumorally injected with either 10^8 PFU of OBP-301 or PBS on days 10, 12, and 14 after tumor inoculation. Primary HT29 tumors were surgically removed on day 15. The relative amount of HT29 tumor cells in mouse lymph nodes isolated on day 35 was assessed by the *Alu*PCR assay (see Figure, Supplemental Digital Content 9, available at: http://links.lww.com/SLA/A46, which illustrates schematic procedures of quantitative PCR evaluation). Note that the preoperative intratumoral administration of OBP-301 significantly (single asterisk: $P < 0.05$) reduced the number of metastatic tumor cells as compared with untreated or surgically treated mice. C, External images of orthotopic HT29 tumor-bearing *nu/nu* mice before and after surgical removal of the primary tumor. D, Macroscopic appearance of the tumor bed after surgical resection of the primary tumor, and the excised HT29 tumor.

of this molecular imaging method.[15,23] It has been reported that the fiber-modified adenovirus serotype 5 (Ad5) and the adenovirus vector based on another serotype such as 35 efficiently transduce exogenous genes into hematopoietic cells, including stem cells; the unmodified Ad5, however, could rarely infect these cells because of the lack of the coxsackievirus and adenovirus receptor expression.[24] Indeed, Ad5-based OBP-301 had no apparent effects on the viability of lymphocytes in vitro. These results suggest that normal lymphocytes in the regional lymph nodes could be strictly protected from OBP-301-induced oncolysis, because lymphocytes are not permissive for OBP-301 infection and viral replication is also unlikely to occur in normal cells due to their low telomerase activity.[25]

Previously, we used serial tissue sections of mouse lymph nodes stained with hematoxylin and eosin to detect microscopic metastasis; this time-consuming technique, however, is not quantitative.[15,23] To quantify the few metastatic human tumor cells in a background of large numbers of mouse host cells, a simple real-time *Alu*PCR assay was developed in the current study. This human-specific amplification method enabled us to detect human tumor cells in a linear range of 10^3 to 10^8 cells/sample and monitor the time-dependent exponential growth of spontaneous lymph node metastasis from orthotopic colorectal tumor xenografts (Fig. 3). In accordance with the histologically confirmed results, the *Alu*PCR assay indicated that intratumoral injection of OBP-301 into the primary tumors significantly inhibited lymph node metastasis with high levels of viral replication (Figs. 4, 5). We also used the previously established OBP-401-mediated in vivo imaging in combination with a 3-dimensional optical detection system (IVIS 200) to demonstrate a significant suppressive effect of OBP-301 against lymph node metastasis (Fig. 6). The fact that 2 independent and highly sensitive approaches showed comparable results suggests a potent in vivo purging effect of oncolytic virotherapy on regional lymph nodes.

Currently, surgery and radiation are the most effective and clinically reliable local management strategies for human malignancies including lymphatic metastases. Indeed, ionizing radiation targeting the lower half of the mouse body including primary tumors and the para-aortic lymphatic area significantly inhibited lymph node metastasis (Fig. 7A), although the systemic toxicity such as the body weight loss was remarkable in irradiated mice compared with mice treated with OBP-301 (data not shown). In fact, a total body irradiation at a dose of 10 Gy has been reported to be lethal in mice because of acute radiation syndromes involving the hematopoietic system and gastrointestinal tract.[26] In this regard, our data clearly indicate that regional oncolytic virotherapy might be more simple and safe than radiotherapy as a treatment for metastatic lymph nodes. We also assessed the effect of surgical resection of primary rectal tumors on lymph node metastasis. Unexpectedly, metastatic tumor cells in the lymph nodes considerably increased after surgical removal of primary tumors, presumably due to the excessive load to the host. Another possible explanation of this phenomenon includes a decrease in angiogenic inhibitors such as angiostatin and endostatin secreted from the primary tumor mass.[27] In contrast, intratumoral injection of OBP-301 prior to surgical resection significantly inhibited lymph node metastasis (Fig. 7B), suggesting that, although the surgical procedure itself has the potential to promote regional metastasis, the preoperative treatment with OBP-301 may prevent this undesirable event.

CONCLUSION

The highly sensitive PCR assay targeting the human *Alu* sequence has shown that the oncolytic adenovirus delivered to the

primary tumor site could spread into the regional draining lymphatics, selectively replicate in neoplastic foci, and then reduce the number of tumor cells in metastatic lymph nodes in an orthotopic human colorectal cancer xenograft model. This virus-mediated molecular surgery for lymph node metastasis mimics the clinical scenario of lymphadenectomy; the technique, however, seems to be safer and less invasive. Moreover, we demonstrated that preoperative delivery of OBP-301 into primary tumors prevented the exacerbation of lymph node metastasis by surgical procedures. OBP-301 may offer advantages over other oncolytic viruses targeting lymphatic metastasis, as its safety profile as well as biodistribution pattern after intratumoral delivery have already been confirmed in a phase I clinical trial for various types of solid tumors.[14] The current study provides evidence for the in vivo purging effect of OBP-301 in regional lymph nodes that is sufficiently reliable to support this approach. Thus, phase II studies of telomerase-specific virotherapy targeting lymph node metastasis in human cancer patients are warranted.

ACKNOWLEDGMENTS

The authors thank Daiju Ichimaru (Oncolys BioPharma, Inc.) for the helpful discussion. The authors also thank Tomoko Sueishi and MitsukoYokota for the excellent technical support.

REFERENCES

1. Maehara Y, Oshiro T, Endo K, et al. Clinical significance of occult micrometastasis lymph nodes from patients with early gastric cancer who died of recurrence. *Surgery*. 1996;119:397–402.
2. Rivadeneira DE, Simmons RM, Christos PJ, et al. Predictive factors associated with axillary lymph node metastases in T1a and T1b breast carcinomas: analysis in more than 900 patients. *J Am Coll Surg*. 2000;191:1–6.
3. Chang GJ, Rodriguez-Bigas MA, Skibber JM, et al. Lymph node evaluation and survival after curative resection of colon cancer: systematic review. *J Natl Cancer Inst*. 2007;99:433–441.
4. Volpe CM, Koo J, Miloro SM, et al. The effect of extended lymphadenectomy on survival in patients with gastric adenocarcinoma. *J Am Coll Surg*. 1995;181:56–64.
5. Harrison LE, Karpeh MS, Brennan MF. Extended lymphadenectomy is associated with a survival benefit for node-negative gastric cancer. *J Gastrointest Surg*. 1998;2:126–131.
6. Sasako M, Sano T, Yamamoto S, et al. D2 lymphadenectomy alone or with para-aortic nodal dissection for gastric cancer. *N Engl J Med*. 2008;359:453–462.
7. Gotoda T, Sasako M, Ono H, et al. Evaluation of the necessity for gastrectomy with lymph node dissection for patients with submucosal invasive gastric cancer. *Br J Surg*. 2001;88:444–449.
8. Liu TC, Galanis E, Kirn D. Clinical trial results with oncolytic virotherapy: a century of promise, a decade of progress. *Nat Clin Pract Oncol*. 2007;4:101–117.
9. Kirn DH, Thorne SH. Targeted and armed oncolytic poxviruses: a novel multi-mechanistic therapeutic class for cancer. *Nat Rev Cancer*. 2009;9:64–71.
10. Fujiwara T. Telomerase-specific virotherapy for human squamous cell carcinoma. *Expert Opin Biol Ther*. 2009;9:321–329.
11. Kawashima T, Kagawa S, Kobayashi N, et al. Telomerase-specific replication-selective virotherapy for human cancer. *Clin Cancer Res*. 2004;10:285–292.
12. Umeoka T, Kawashima T, Kagawa S, et al. Visualization of intrathoracically disseminated solid tumors in mice with optical imaging by telomerase-specific amplification of a transferred green fluorescent protein gene. *Cancer Res*. 2004;64:6259–6265.
13. Taki M, Kagawa S, Nishizaki M, et al. Enhanced oncolysis by a tropism-modified telomerase-specific replication-selective adenoviral agent OBP-405 (Telomelysin-RGD). *Oncogene*. 2005;24:3130–3140.
14. Fujiwara T, Tanaka N, Numunaitis JJ, et al. Phase I trial of intratumoral administration of OBP-301, a novel telomerase-specific oncolytic virus, in patients with advanced solid cancer: evaluation of biodistribution and immune response. *J Clin Oncol*. 2008;26:3572.
15. Kishimoto H, Kojima T, Watanabe Y, et al. In vivo imaging of lymph node metastasis with telomerase-specific replication-selective adenovirus. *Nat Med*. 2006;12:1213–1219.
16. Johnson M, Huyn S, Burton J, et al. Differential biodistribution of adenoviral vector in vivo as monitored by bioluminescence imaging and quantitative polymerase chain reaction. *Hum Gene Ther*. 2006;17:1262–1269.
17. Burton JB, Johnson M, Sato M, et al. Adenovirus-mediated gene expression imaging to directly detect sentinel lymph node metastasis of prostate cancer. *Nat Med*. 2008;14:882–888.
18. Schneider T, Osl F, Friess T, et al. Quantification of human Alu sequences by real-time PCR—an improved method to measure therapeutic efficacy of anti-metastatic drugs in human xenotransplants. *Clin Exp Metastasis*. 2002;19:571–582.
19. Zijlstra A, Mellor R, Panzarella G, et al. A quantitative analysis of rate-limiting steps in the metastatic cascade using human-specific real-time polymerase chain reaction. *Cancer Res*. 2002;62:7083–7092.
20. Umetani N, Giuliano AE, Hiramatsu SH, et al. Prediction of breast tumor progression by integrity of free circulating DNA in serum. *J Clin Oncol*. 2006;24:4270–4276.
21. Kariya Y, Kato K, Hayashizaki Y, et al. Revision of consensus sequence of human Alu repeats—a review. *Gene*. 1987;53:1–10.
22. Liu TC, Kirn D. Systemic efficacy with oncolytic virus therapeutics: clinical proof-of-concept and future directions. *Cancer Res*. 2007;67:429–432.
23. Kurihara Y, Watanabe Y, Onimatsu H, et al. Telomerase-specific virotheranostics for human head and neck cancer. *Clin Cancer Res*. 2009;15:2335–2343.
24. Kawabata K, Sakurai F, Koizumi N, et al. Adenovirus vector-mediated gene transfer into stem cells. *Mol Pharm*. 2006;3:95–103.
25. Hiyama K, Hirai Y, Kyoizumi S, et al. Activation of telomerase in human lymphocytes and hematopoietic progenitor cells. *J Immunol*. 1995;155:3711–3715.
26. Burdelya LG, Krivokrysenko VI, Tallant TC, et al. An agonist of toll-like receptor 5 has radioprotective activity in mouse and primate models. *Science*. 2008;320:226–230.
27. Folkman J. Role of angiogenesis in tumor growth and metastasis. *Semin Oncol*. 2002;29:15–18.

Research Article

Molecular Cancer Therapeutics

Preclinical Evaluation of Differentially Targeting Dual Virotherapy for Human Solid Cancer

Ryo Sakai[1], Shunsuke Kagawa[1,2], Yasumoto Yamasaki[1], Toru Kojima[1], Futoshi Uno[1,2], Yuuri Hashimoto[1,3], Yuichi Watanabe[1,3], Yasuo Urata[3], Noriaki Tanaka[1], and Toshiyoshi Fujiwara[1,2]

Abstract

Multimodal approaches combining drugs that differentially function is the most popular regimen for treating human cancer. Understanding the molecular mechanisms underlying the synergistic, potentiative, and antagonistic effects of drug combinations could facilitate the discovery of novel efficacious combinations. We previously showed that telomerase-specific replication-competent adenovirus (Telomelysin, OBP-301), in which the human telomerase reverse transcriptase promoter controls the adenoviral E1 gene expression, induces a selective antitumor effect in human cancer cells. Here, using E1-deleted replication-deficient adenovirus expressing the p53 tumor suppressor gene (Advexin, Ad-p53) and OBP-301, we investigate how these adenoviruses that kill tumor cells with different mechanisms could work in combination on human cancer. We found that E1-deficient Ad-p53 could kill cancer cells more efficiently in the presence of OBP-301 than Ad-p53 alone or OBP-301 alone, because Ad-p53 could become replication-competent by being supplied adenoviral E1 from coinfected OBP-301 in trans. Ad-p53 plus OBP-301 induced high levels of p53 protein expression without p21 induction, resulting in apoptotic cell death documented by active caspase-3 expression with a cytometric bead array and an increased subdiploid apoptotic fraction of the cell cycle. For *in vivo* evaluation, nude mice xenografted with human lung tumors received intratumoral injection of OBP-301 and/or Ad-p53. Analysis of the growth of implanted tumors showed an enhanced antitumor effect in combination therapy. Our data show that Ad-p53 in combination with OBP-301 induces not only oncolytic but also apoptotic cancer cell death and enhances antitumor activity *in vitro* and *in vivo*, providing potential merits as a multimodal treatment for human cancer. *Mol Cancer Ther; 9(6); 1884–93. ©2010 AACR.*

Introduction

Combining antineoplastic agents with different mechanisms of action has resulted in many effective regimens in cancer therapy. For example, biochemical modulation of 5-fluorouracil, one of the most active single agents presently available, with the reduced folate leucovorin has significantly improved overall response rates in the 25% to 30% range (1). To successfully achieve synergistic effects, we need to elucidate the biochemical and/or molecular mechanisms underlying the drug interaction. Recent advances in understanding the molecular mechanisms of carcinogenesis allow us to develop a number of molecularly targeted therapies. Most agents have been developed to target specific molecules which are essential for the acquisition of malignant phenotypes such as proliferation, invasion, and metastasis.

Gene- and vector-based therapies, which have long been viewed as unsuccessful, have been greatly rejuvenated by its combination with other modalities including chemotherapy and radiotherapy (2, 3). It also remains possible to increase the therapeutic benefit by combining virotherapies having different targets. Ad-p53 (Advexin, Ad5CMV-p53) consists of an E1-deleted replication-deficient type 5 adenoviral vector expressing the human wild-type p53 tumor suppressor gene under the control of a cytomegalovirus promoter. p53 is the most commonly mutated gene in human cancer (4, 5), and p53 gene therapy using Ad-p53 is currently in clinical trials as a cancer therapy (6–9); however, a number of limitations have led to the suboptimal efficacy of existing gene therapies. One reason is that replication-deficient adenoviruses infect only a small portion of the tumor and are not able to spread over the tumor entirely. To improve viral spread in tumor conferring specificity of infection, replication-competent adenoviruses have been investigated (10–12).

Authors' Affiliations: [1]Department of Gastroenterological Surgery, Okayama University Graduate School of Medicine, Dentistry, and Pharmaceutical Sciences, [2]Center for Gene and Cell Therapy, Okayama University Hospital, Okayama, Japan; and [3]Oncolys BioPharma, Inc., Tokyo, Japan

Corresponding Author: Toshiyoshi Fujiwara, Department of Gastroenterological Surgery, Okayama University Graduate School of Medicine, Dentistry, and Pharmaceutical Sciences, 2-5-1 Shikata-cho, Kita-ku, Okayama 700-8558, Japan. Phone: 81-86-235-7257; Fax: 81-86-221-8775. E-mail: toshi_f@md.okayama-u.ac.jp

doi: 10.1158/1535-7163.MCT-10-0205

We previously developed a telomerase-specific, replication-competent adenovirus (Telomelysin, OBP-301), in which the human telomerase reverse transcriptase (hTERT) promoter element drives the adenoviral E1 gene, and induced a selective antitumor effect in human cancer cells (13–17). Telomerase is a ribonucleoprotein complex responsible for the complete replication of chromosomal ends (18). Many studies have shown the expression of telomerase activity in more than 85% of human cancers (19), but only in few normal somatic cells (20). Telomerase activation is considered a critical step in carcinogenesis and its activity is closely correlated with hTERT expression (21). Although virotherapy using OBP-301 as a monotherapy is currently being evaluated in clinical trials (22), multimodal strategies to enhance antitumor efficacy *in vivo* might be essential for a successful clinical outcome.

As a replication-deficient adenovirus could replicate in cancer cells and enhance the anticancer effect when cotransfected with a replication-competent adenovirus that could produce E1 proteins, we reasoned that combined treatment with Ad-p53 and OBP-301 might offer a way to more efficiently kill human tumor cells. In the present study, we investigated the synergistic effects of Ad-p53 combined with OBP-301 both *in vitro* and *in vivo*.

Materials and Methods

Cell lines and cell cultures

The human non–small cell lung cancer cell line H1299, which has a homozygously deleted p53, and the human colorectal carcinoma cell line SW620, which contains mutated p53, were propagated in monolayer culture in RPMI 1640 supplemented with 10% FCS, 100 units/mL of penicillin, and 100 μg/mL of streptomycin.

Recombinant adenoviruses

The recombinant replication-selective, tumor-specific adenovirus vector OBP-301 (Telomelysin), in which the hTERT promoter element drives the expression of E1A and E1B genes linked with an IRES, was constructed and characterized previously (16). Replication-deficient adenoviral vectors containing human wild-type p53 cDNA (Ad-p53) and β-galactosidase cDNA (Ad-lacZ) were also used (23). These viruses were purified by $CsCl_2$ step gradient ultracentrifugation followed by $CsCl_2$ linear

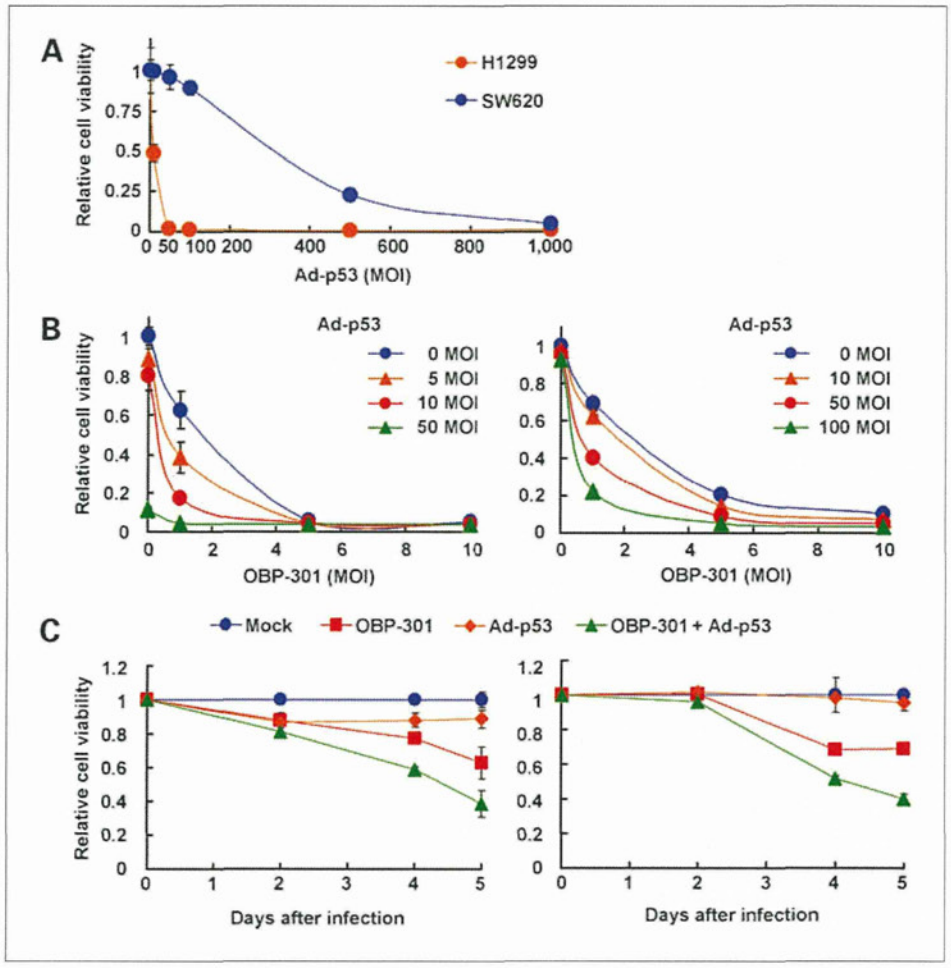

Figure 1. A, effect of Ad-p53 on human cancer cell lines. H1299 and SW620 cells were infected with 0, 10, 50, 100, 500, and 1,000 MOIs of Ad-p53. Cell viability was assessed by XTT assay 5 d after infection. B, dose-response analysis of cell viability in combination therapy. H1299 (left) and SW620 (right) cells were treated with the indicated MOIs of Ad-p53, OBP-301, or a combination of both simultaneously. The cell-killing effect was evaluated by XTT assay 5 d after infection. C, time course analysis of cell viability in combination therapy. H1299 (left) and SW620 (right) cells were treated with 1 MOI of OBP-301, 5 MOI (for H1299) or 50 MOI (for SW620) of Ad-p53, or a combination of both at the same time. Cell viability was assessed by XTT assay 2, 4, and 5 d after infection. Bars, SD.

gradient ultracentrifugation, and their titers were determined by plaque assay in the 293 cells.

Cell proliferation assay

Cells were seeded at 1,000 cells/well in 96-well plate and infected with OBP-301, Ad-p53, or OBP-301 and Ad-p53 simultaneously at the indicated multiplicities of infection (MOI) 18 to 20 hours later. Cell viability was assessed at the indicated times after adenoviral infection using sodium 3′-[1-(phenylaminocarbonyl)-3,4-tetrazolium]-bis(4-methoxy-6-nitro) benzene sulfonic acid hydrate (XTT) assay with the Cell Proliferation Kit II (Roche Molecular Biochemicals) according to the protocol provided by the manufacturer.

Western blot analysis

The primary antibodies against p53 (Ab-2; Calbiochem), p21 (EA10; Oncogene Science), β-actin (AC-15; Sigma Chemical, Co.), and peroxidase-linked secondary antibody (Amersham) were used. Cells were washed twice in cold PBS and collected then lysed in lysis buffer [10 mmol/L Tris (pH 7.5), 150 mmol/L NaCl, 50 mmol/L NaF, 1 mmol/L EDTA, 10% glycerol, and 0.5% NP40] containing proteinase inhibitors (0.1 mmol/L phenylmethylsulfonyl fluoride and 0.5 mmol/L Na_3VO_4). After 20 minutes on ice, the lysates were spun at 14,000 rpm in a microcentrifuge at 4°C for 5 minutes. The supernatants were used as whole cell extracts. Protein concentration was determined using the Bio-Rad protein determination method (Bio-Rad). Equal amounts of proteins were boiled for 5 minutes and electrophoresed under reducing conditions in 4% to 12% (w/v) polyacrylamide gels. Proteins were electrophoretically transferred to Hybond polyvinylidene difluoride transfer membranes (Amersham Life Science) and incubated with the primary antibody followed by peroxidase-linked secondary antibody. An Amersham ECL chemiluminescent western system (Amersham) was used to detect secondary probes.

Human apoptosis cytometric bead array for active caspase-3

Caspase-3 activation was quantitated using the Human Apoptosis Cytometric Bead Array kit (Becton Dickinson) according to the instructions of the manufacturer. Briefly, cell lysates were incubated with cytometric caspase-3 capture beads coated with antibody specific for caspase-3 and a secondary antibody specific for the cleaved site of active caspase-3 conjugated to phycoerythrin. Cytometric bead/caspase-3 conjugates were analyzed by flow cytometry using a FACSCalibur (Becton Dickinson). Flow cytometry measures the amount of active caspase-3 attached to beads. Becton Dickinson Cytometric Bead Array software was used to analyze beads and transform data from samples. Sample data

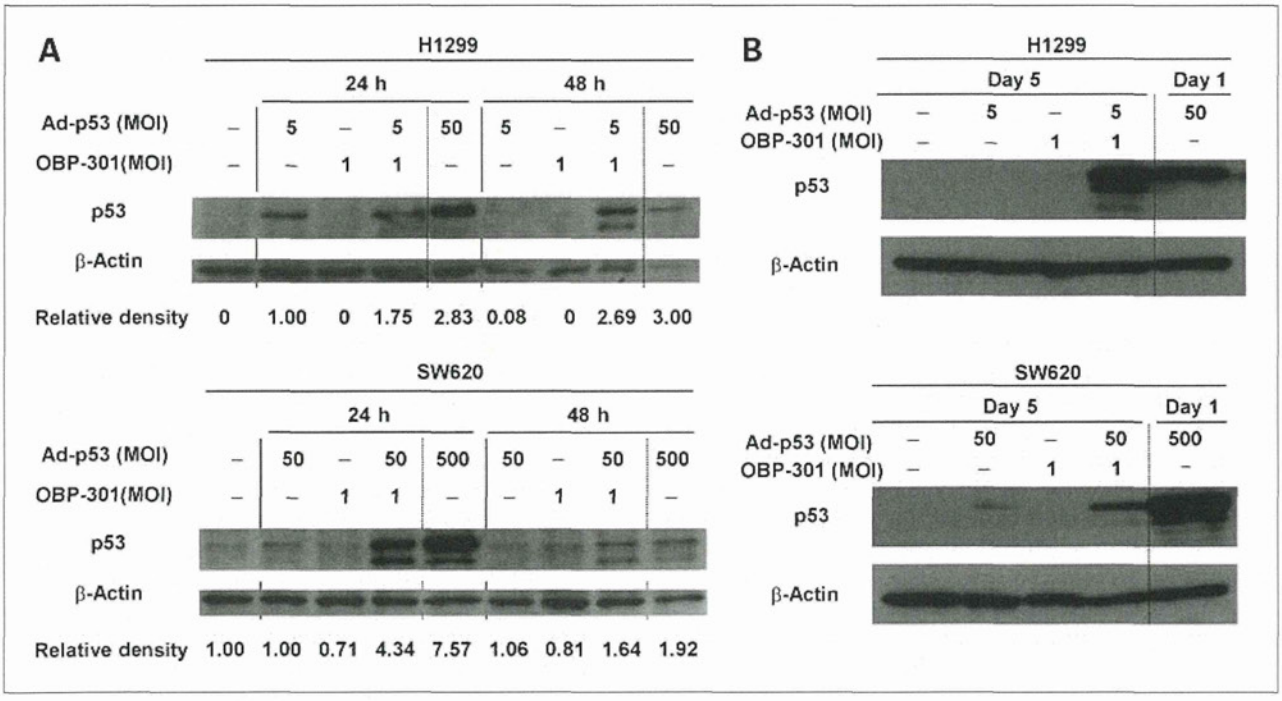

Figure 2. Expression of p53 in combination therapy of Ad-p53 and OBP-301. H1299 and SW620 cells were infected with the indicated viruses and harvested at the indicated time. Cell lysates were subjected to immunoblot analysis for p53 and β-actin. H1299 cells infected with 50 MOI of Ad-p53 and SW620 cells infected with 500 MOI of Ad-p53 were used as a positive control for apoptosis. A, cells were harvested in the early phase (24 and 48 h after infection). p53 expression level was quantified by densitometric scanning using NIH Image software and normalization by dividing the β-actin signal. The background was subtracted and corrected so that the control became 0, because H1299 cells were p53-null. B, cells were harvested in the late phase (5 d after infection).

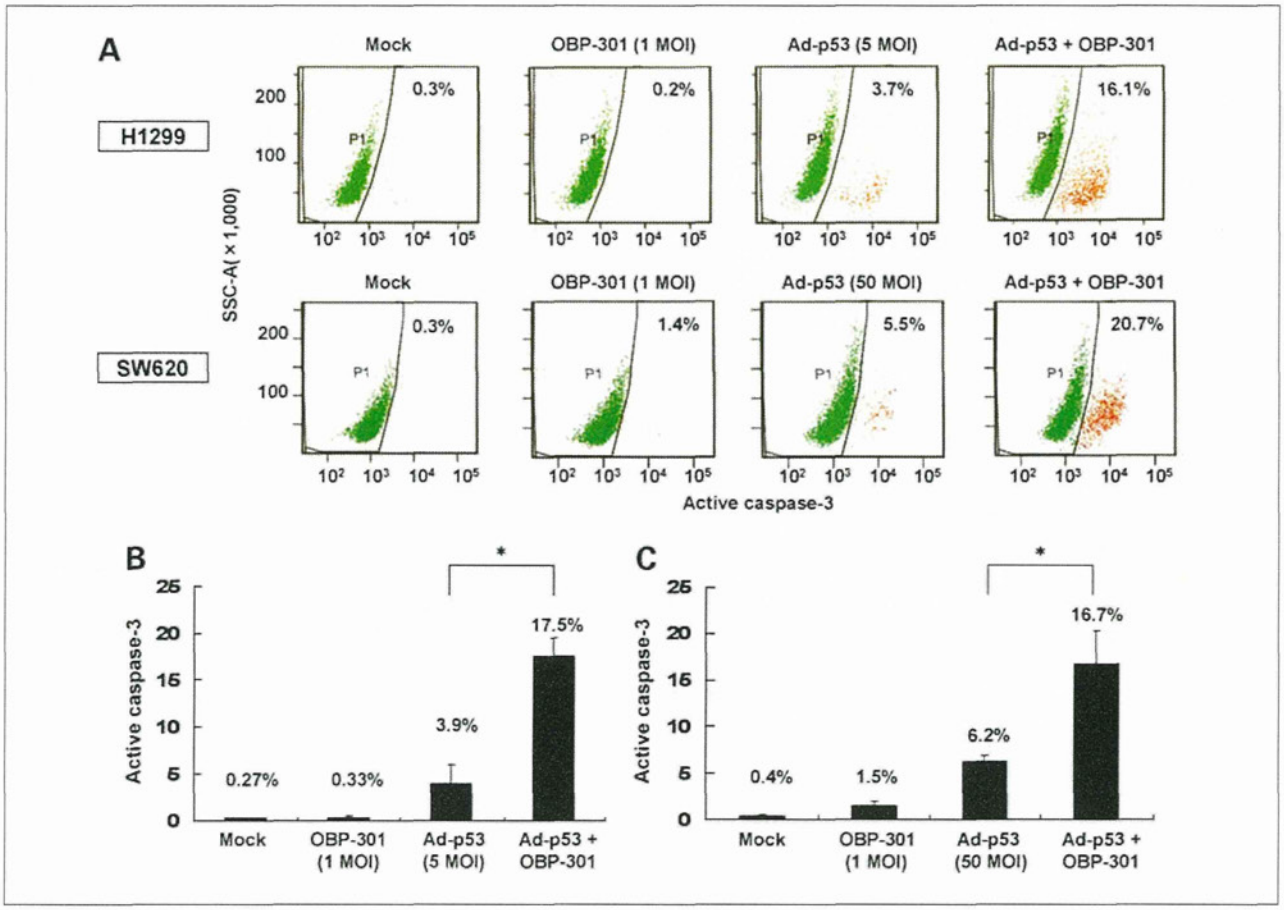

Figure 3. Induction of apoptosis in H1299 and SW620 cells following infection with Ad-p53 plus OBP-301. H1299 and SW620 cells were infected with the indicated MOIs of OBP-301, Ad-p53, or a combination of both simultaneously. Caspase-3 activation was quantitated using the cytometric bead array (CBA) assay 48 h after infection. A, representative flow cytometric images are shown. B and C, active caspase-3 expression was significantly increased after infection with Ad-p53 plus OBP-301 in H1299 (B) and SW620 (C) cells. Columns, mean of three experiments; bars, SE. *, $P < 0.01$, statistical significance (Student's t test).

was normalized with specific protein standards to provide quantification of the proteins of interest.

In vitro replication assay

H1299 cells were infected with OBP-301 (1 MOI), Ad-p53 (5 MOI), OBP-301 (1 MOI) + Ad-p53 (5 MOI), or OBP-301 (1 MOI) + Ad-lacZ (5 MOI) for 24 hours after seeding for 2 hours. Following the removal of virus inocula, the cells were further incubated at 37°C, trypsinized, and harvested at 2, 24, 48, and 72 hours after infection. DNA purification was done using QIAmp DNA mini kit (Qiagen, Inc.). The E1A and p53 DNA copy numbers were determined by quantitative real-time PCR using a LightCycler instrument and LightCycler-DNA Master SYBR Green I (Roche Diagnostics).

Cell cycle analysis

Cells treated with various concentrations of OBP-301, Ad-p53, or a combination of both were harvested in 0.125% trypsin, washed twice in PBS with 2% FCS. After centrifugation, 1×10^6 cells were resuspended in 70% ethanol at 4°C overnight. Cells were washed twice in PBS. After centrifugation, the pellet was resuspended in 0.25 μg/mL of RNase A for 30 minutes at 37°C. The samples were then stained with 50 μg/mL of propidium iodide and incubated at 4°C for 30 minutes. Cell cycle analysis was determined by FACSCalibur flow cytometer using FlowJo software (TreeStar, Inc.).

In vivo human tumor model

H1299 cells (7.5×10^6 cells/mouse) were injected s.c. into the flank of 5-week-old female BALB/c *nu/nu* mice and permitted to grow to 4 to 10 mm in diameter. At that time, the mice were randomly assigned into six groups, and a 50 μL solution containing Ad-p53 [1×10^9 plaque-forming units (pfu)], OBP-301(1×10^7 pfu), OBP-301 (1×10^7 pfu) + Ad-p53 (1×10^8 pfu), or Ad-lacZ (1×10^8 pfu), Ad-p53 (1×10^8 pfu) + Ad-lacZ (1×10^7 pfu), or PBS was injected into the tumor for three cycles every 2 days. The perpendicular diameter of each tumor was measured every 3 or 4 days, and tumor volume was calculated using the following formula:

tumor volume (mm^3) = $a \times b^2 \times 0.5$, where a is the longest diameter, b is the shortest diameter and 0.5 is a constant to calculate the volume of an ellipsoid. The experimental protocol was approved by the Ethics Review Committee for Animal Experimentation of Okayama University School of Medicine.

Statistical analysis

The statistical significance of the differences in the *in vitro* and *in vivo* antitumor effects of viruses was determined by using the (two-tailed) Student's t test.

Results

Enhanced antitumor effect of OBP-301 plus Ad-p53 in human cancer cell lines *in vitro*

To achieve optimum antitumor effect, Ad-p53 at the MOI of 50 and 500 was needed in H1299 and SW620 cells, respectively (Fig. 1A). We have previously confirmed that these cells expressed detectable hTERT mRNA (13, 14). To examine the potential interaction of Ad-p53 with OBP-301, we did a dose-response analysis of the cell-killing effect at various doses in H1299 and SW620 cells. Ad-p53 at 5 or 50 MOI could have little antitumor effect in H1299 and SW620 cells, respectively. Combination therapy with 1 MOI of OBP-301 plus Ad-p53 resulted in more cell killing than OBP-301 alone or Ad-p53 alone in both cells (Fig. 1B). In contrast, OBP-301 plus Ad-lacZ did not increase the antitumor effect (data not shown). We next examined a time course analysis of the cell-killing effect. The antitumor effect of Ad-p53 plus OBP-301 was augmented after 4 days of infection (Fig. 1C). To determine whether the timing of administration of the adenoviruses affected the combined cytotoxic effect, H1299 and SW620 cells were treated with Ad-p53 24 hours after infection or synchronously with OBP-301. The results showed no apparent differences in cytotoxic activity by the treatment schedules (data not shown).

Increased expression of p53 by cotransduction with OBP-301 and Ad-p53

To explore the effect of the combination of Ad-p53 and OBP-301, the expression levels of p53 protein were compared by immunoblotting analyses at 24 and 48 hours after infection. By cotransduction with Ad-p53 and OBP-301, the expression of p53 was 33.6-fold higher in H1299 cells at 48 hours and 4.34-fold higher in SW620

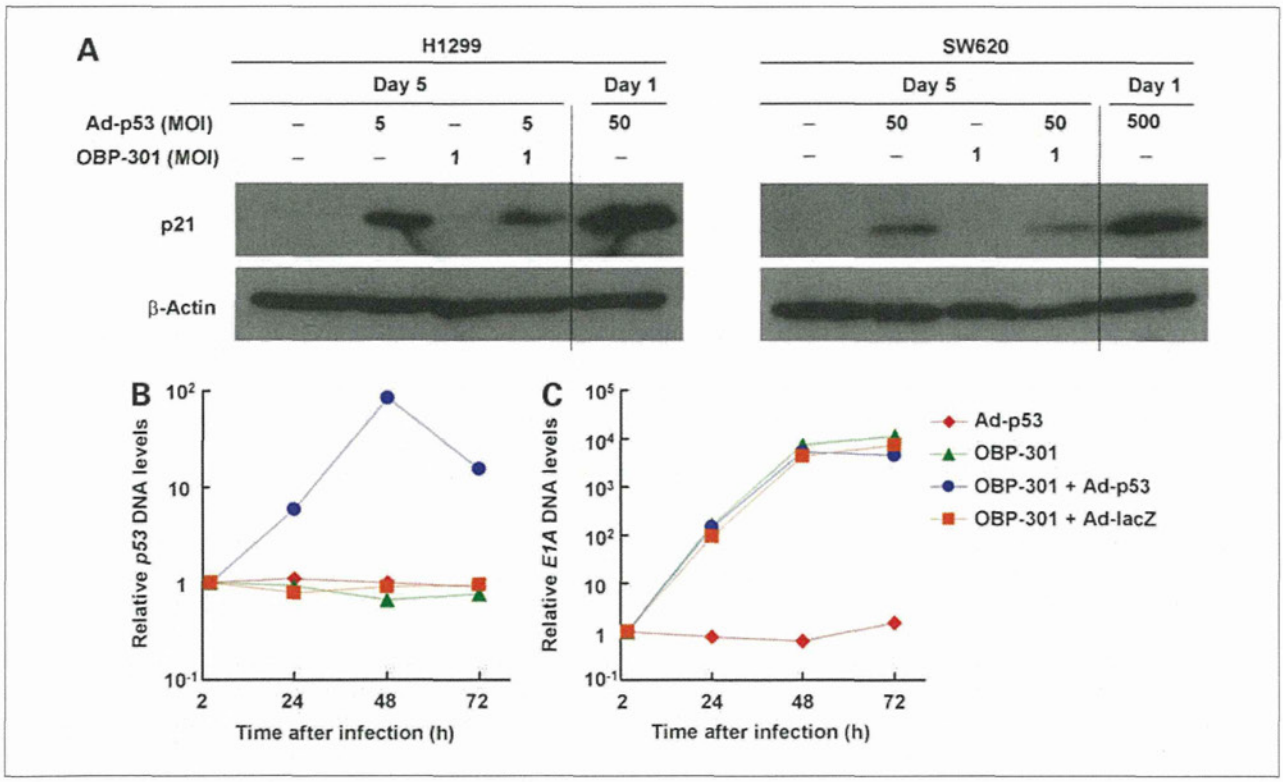

Figure 4. A, expression of p53 downstream mediator p21. H1299 and SW620 cells were infected with the indicated viruses and harvested at the indicated times. Cell lysates were subjected to immunoblot analyses for p21 and β-actin. H1299 cells infected with 50 MOI of Ad-p53 and SW620 cells infected with 500 MOI of Ad-p53 were used as a positive control for p21 induction. B and C, assessment of viral DNA replication in H1299 cells. H1299 cells were infected with OBP-301 (1 MOI), Ad-p53 (5 MOI), OBP-301 (1 MOI) + Ad-p53 (5 MOI), or OBP-301 (1 MOI) + Ad-lacZ (5 MOI) for 2 h. Following the removal of virus inocula, the cells were further incubated at 37°C, trypsinized, and harvested at 2, 24, 48, and 72 h after infection. Extracted DNA was subjected to real-time PCR assay for p53 DNA (B) and E1A DNA (C).

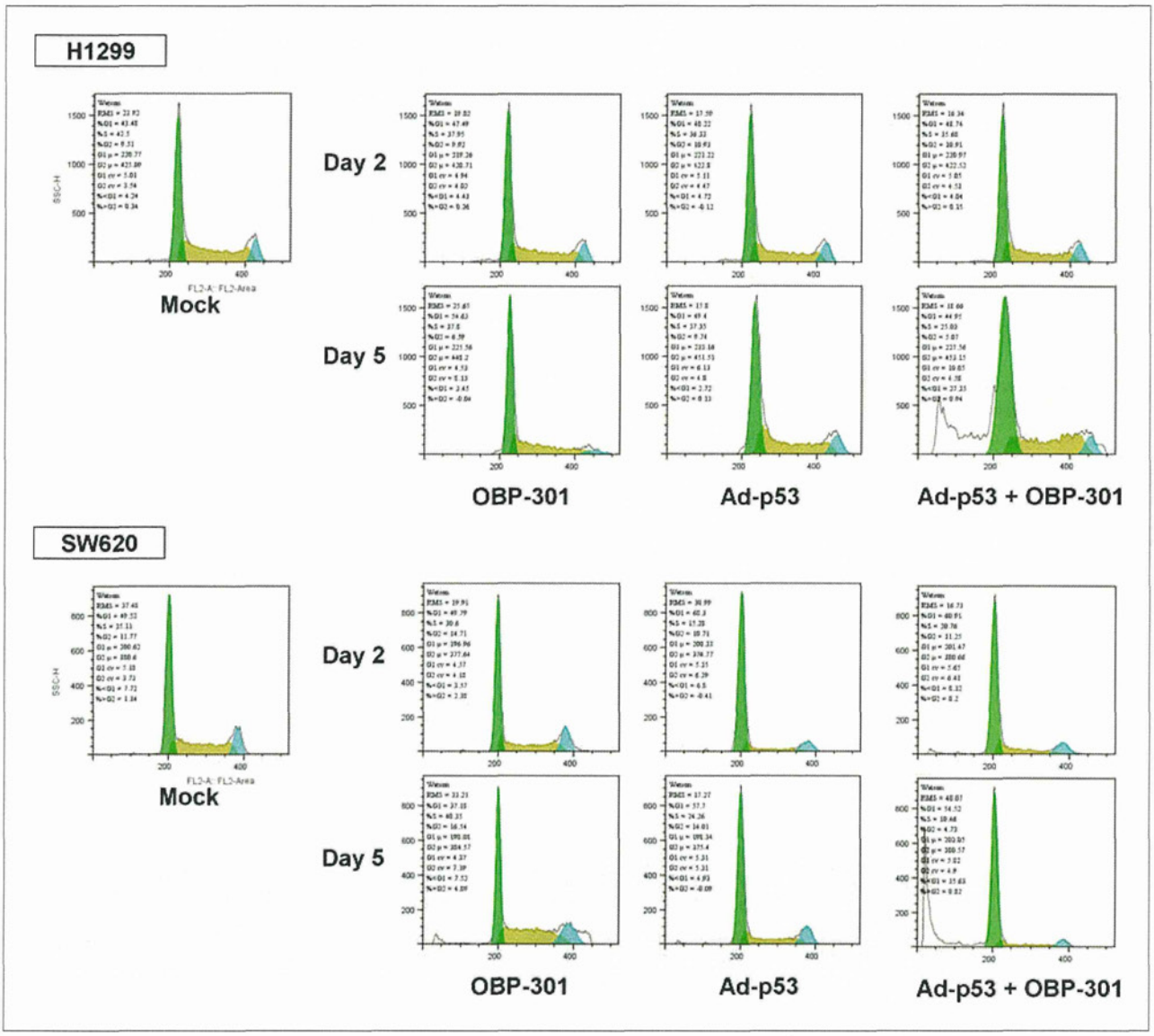

Figure 5. H1299 cells were infected with 1 MOI of OBP-301, 5 MOI of Ad-p53, or a combination of both and harvested on days 2 and 5. SW620 cells were infected with 1 MOI of OBP-301, 50 MOI of Ad-p53, or a combination of both and harvested on days 2 and 5. Cells were stained with propidium iodide. Then, cell cycle analysis was determined by the fluorescence-activated cell sorter (FACSCalibur) flow cytometer.

cells at 24 hours than by Ad-p53 alone (Fig. 2A). The augmented expression of p53 was maintained in cotransduced cells with both adenoviruses on day 5 (Fig. 2B). The prolonged upregulation of p53 suggests that Ad-p53 replicates in cancer cells by E1 protein supplied by cotransduced OBP-301, although the pattern of increased p53 expression was different between H1299 and SW620 cells. These cells expressed equivalent levels of coxsackievirus and adenovirus receptor (15); p53-null H1299 cells were, however, more sensitive to Ad-p53 compared with SW620 cells containing mutated p53, as shown in Fig. 1A, suggesting that Ad-p53 induced rapid apoptosis within 48 hours in infected H1299 cells and, therefore, p53 expression declined at 48 hours after infection. In contrast, as Ad-p53 could replicate and infect more H1299 cells in the presence of OBP-301, the level of p53 expression increased after coinfection of Ad-p53 and OBP-301.

Combined treatment of OBP-301 plus Ad-p53 more efficiently induced apoptosis

Overexpression of p53 is known to induce apoptosis in most cancer cells. We hypothesized that the enhanced antitumor effect of Ad-p53 plus OBP-301 would result in elevated apoptotic cell death. Two days after infection, combined treatment of Ad-p53 plus OBP-301 induced significantly elevated levels of active caspase-3, whereas a low dose of Ad-p53 alone did not (Fig. 3). Moreover, interestingly, the expression level of p21, which is a

downstream target of p53 in combination therapy with OBP-301 and Ad-p53, was lower than in low doses of Ad-p53 alone (Fig. 4A).

p53 DNA copy number is significantly amplified in combination therapy with OBP-301 and Ad-p53, whereas p53 does not impair the replication of OBP-301

Then we examined the p53 DNA levels in H1299 cells. The amplification of p53 DNA in the cells treated with Ad-p53 plus OBP-301 by one to two orders of magnitude was observed (Fig. 4B). These results suggest that Ad-p53 actually replicates by using the E1 protein supplied by OBP-301, which is consistent with increased expression of p53 protein (Fig. 2A). In this combination treatment, proapoptotic p53 expression might impair the replication of oncolytic virus because of premature early cell death provoked by p53. Therefore, we examined the effect of p53 on the replication of OBP-301 by quantitative real-time PCR analysis. H1299 cells were infected with OBP-301 and/or Ad-p53. Cells were harvested 2, 24, and 48 hours after infection, and extracted DNA were subjected to the assay. As shown in Fig. 4C, the presence of Ad-p53 did not impair the replication of OBP-301.

Augmentation of apoptosis in human tumor cells after coinfection with Ad-p53 and OBP-301

We next did a cell cycle analysis in H1299 and SW620 cells on days 2 and 5 after infection. Neither group showed any differences between treatment 2 days after infection; however, a sub-G_1 population (an apoptotic cell population) was markedly increased in H1299 and SW620 cells infected with Ad-p53 plus OBP-301 after 5 days of infection, whereas OBP-301 or Ad-p53 alone did not increase apoptosis (Fig. 5; Table 1). These results were compatible with those of the time course analyses (Fig. 1C), suggesting that the augmented antitumor effect of combined treatment of Ad-p53 and OBP-301 was due to enhanced apoptotic cancer cell death.

Antitumor effect of OBP-301 plus Ad-p53 in human tumor xenografts

Based on the *in vitro* combination effect of Ad-p53 and OBP-301, the *in vivo* therapeutic efficacy of H1299 tumors was further assessed. Mice bearing H1299-xenografted tumors measuring 4 to 10 mm in diameter received intratumoral injection of Ad-p53 at a dose of 1×10^8 pfu and OBP-301 at a dose of 1×10^7 pfu, singly or in combination every 2 days for three cycles starting at day 0. As shown in Fig. 6, Ad-p53 alone and Ad-p53 + Ad-lacZ had no apparent antitumor effect, but OBP-301 alone resulted in significant tumor suppression compared with controls ($P < 0.05$). OBP-301 plus Ad-lacZ did not improve the tumor suppression compared with OBP-301 alone ($P > 0.05$). Nevertheless, the combination of OBP-301 plus Ad-p53 produced a more profound and significant inhibition of tumor growth compared with OBP-301 alone or OBP-301 plus Ad-lacZ ($P < 0.05$).

Table 1. Cell cycle analysis following infection with OBP-301, Ad-p53, or Ad-p53 plus OBP-301 in H1299 and SW620 cells

Cell lines	Days	Treatments	Cell cycle distribution (%)			
			Sub-G_0-G_1	G_0-G_1	S	G_2-M
H1299		Mock	4.51	43.48	42.5	9.51
	Day 2	OBP-301	4.64	47.49	37.95	9.92
		Ad-p53	4.52	48.22	36.33	10.93
		Ad-p53 + OBP-301	4.67	48.74	35.68	10.91
	Day 5	OBP-301	0.98	54.63	37.8	6.59
		Ad-p53	3.51	49.4	37.35	9.74
		Ad-p53 + OBP-301	24.95	44.95	25.03	5.07
SW620		Mock	3.06	49.52	35.11	11.77
	Day 2	OBP-301	4.9	49.79	30.6	14.71
		Ad-p53	5.71	68.3	15.28	10.71
		Ad-p53 + OBP-301	7.08	60.91	20.76	11.25
	Day 5	OBP-301	5.93	37.18	40.35	16.54
		Ad-p53	4.03	57.7	24.26	14.01
		Ad-p53 + OBP-301	30.29	54.52	10.46	4.73

NOTE: H1299 cells were infected with 1 MOI of OBP-301, 5 MOI of Ad-p53, or a combination of both and harvested on days 2 and 5. SW620 cells were infected with 1 MOI of OBP-301, 50 MOI of Ad-p53, or a combination of both and harvested on days 2 and 5. Cell cycle analysis was determined by the fluorescence-activated cell sorter (FACSCalibur) flow cytometer.